THESIS

COMPARISON OF MICROPHYSICAL AND TOPOGRAPHICAL INFLUENCES ON WARM SEASON STORM ELECTRIFICATION BETWEEN SUBTROPICAL SOUTH AMERICA AND COLORADO

Submitted by

Mitchell L. Gregg

Department of Atmospheric Science

In partial fulfillment of the requirements

For the Degree of Master of Science

Colorado State University

Fort Collins, Colorado

Summer 2025

Master's Committee:

Advisor: Kristen L. Rasmussen

Russ S. Schumacher
V. Chandrasekar
Ryan Morrison

ABSTRACT

COMPARISON OF MICROPHYSICAL AND TOPOGRAPHICAL INFLUENCES ON WARM SEASON STORM ELECTRIFICATION BETWEEN SUBTROPICAL SOUTH AMERICA AND COLORADO

Sixteen years of observations from the Tropical Rainfall Measurement Mission (TRMM) satellite's Precipitation Radar were key in identifying subtropical South America in the lee of the Andes as a global hotspot for convection, with frequent back-building over terrain producing intense convection yielding some of the highest lightning flash rates on Earth. These observations motivated the 2018 Remote sensing of Electrification, Lightning, And Mesoscale/microscale Processes with Adaptive Ground Observations (RELAMPAGO) field campaign, which sought to further investigate convection and electrification processes through the deployment of Colorado State University's CHIVO radar and a NASA Lightning Mapping Array (LMA). In 2021, the Preparatory Rockies Experiment for the Campaign in the Pacific ("PRE"-CIP) campaign took place in northern Colorado to study extreme precipitation and convection in the lee of the Rockies, deploying the same CHIVO radar near a permanent LMA network. CHIVO radar observations are used to identify discrete precipitation features and microphysical parameters key to storm electrification for approximately three months during the warm seasons in both Argentina and Colorado. LMA-observed lightning flashes are co-located with these precipitation features, allowing for analysis of the relationships between various microphysical parameters and lightning behavior throughout a storm's lifecycle, in both regions. The continuity in instrumentation,

precipitation feature identification methods, and microphysical/hydrometeor identification calculations across both campaigns allows for the first direct comparison of microphysical drivers to electrification across a spectrum of storm modes between these two regions.

Subtropical South America is characterized by systematically larger and taller convection with higher-altitude lightning flashes. LMA data from both campaigns demonstrates that lightning in Colorado occurs most frequently over the immediate plains east of the Rockies, while in South America, flashes occur more frequently over the foothills, highlighting the critical role of the Sierras de Córdoba, a secondary mountain range east of the Andes, in the back-building of convection observed in this region. Regressions developed between key microphysical parameters and lightning flash rates demonstrate that subtropical South American storms require significantly greater intense echoes and graupel volumes to produce similar lightning flash rates as storms in Colorado, suggesting a characteristic difference in electrification processes and the role and efficiency of microphysical processes between these two regions. The fundamental differences in convective and lightning processes identified between these two regions demonstrates the need for future work to prioritize both microphysical and kinematic drivers in a more diverse sample of climate regions around the world.

TABLE OF CONTENTS

CHAPTER 1

INTRODUCTION

Subtropical South America (SSA) in the lee of the Andes is home to some of the most intense and extreme deep convection on the planet, with 40 dBZ echo top heights frequently exceeding 15 km and production of some of the largest hail on Earth (Zipser et al. 2006, Cecil and Blankenship 2012, Houze et al. 2015). Convective storms are known to initiate and back-build over the local terrain, often growing upscale into large mesoscale convective systems (MCSs; Houze 2004) that eventually move east across the adjacent plains (Romatschke and Houze 2010; Rasmussen and Houze 2011, 2016), producing severe impacts such as flooding, hail, tornadoes, and lightning (Nascimento and Doswell III 2005, Rasmussen et al. 2014). While satellite studies of global lightning activity have long shown the close relationship between convective lightning and topographic forcings, storms that form in the lee of the Andes are some of the most electrically active, with TRMM-observed precipitation features (PFs) in subtropical South America (SSA) having some of the highest flash rates on Earth (Kummerow et al. 1998, Zipser et al. 2006, Albrecht et al. 2016).

The foothills of the Sierras de Córdoba (SDC), a smaller but still prominent secondary mountain range east of the Andes in Argentina, have been shown to play a crucial role in convective initiation and terrain-locked back-building in this region (Rasmussen et al. 2014, Singh et al. 2022). Previous work has found a strong dependence of the height of this topography on the resultant intensity and life cycle of convection downwind (Insel et al. 2010, Rasmussen and Houze 2016, Mulholland et al. 2020, Rocque and Rasmussen 2022). The magnitude of resultant lee

cyclogenesis and moisture transport from the Amazon via the South American Low-Level Jet (SALLJ; Vera et al. 2006, Sasaki et al. 2022) are dependent on this topography, as well as the magnitudes of environmental convective available potential energy (CAPE) and convective inhibition (CIN) across the region. In simulations with lower Andes heights, which more closely resembles the shorter Rockies, both CAPE and CIN decreased, and convection became more widespread and less terrain-locked (Rasmussen and Houze 2016).

The co-location of exceptional convective activity, globally distinct lightning processes, and favorable synoptic weather patterns poses a unique research opportunity. While satellite-based studies have been instrumental in characterizing SSA as a global convective and lightning hotspot, they are inherently limited in what they are able to capture. TRMM's low Earth orbit means that it excels at capturing short moments in time but cannot continuously observe the full convective lifecycle of a given storm, making it challenging to diagnose specific processes that drive its evolution and lightning activity. Motivated by the groundwork laid by spaceborne studies in identifying SSA as a global hotspot for convection and lightning, the Remote Sensing of Electrification, Lightning, and Mesoscale/Microscale Processes with Adaptive Ground Observations (RELAMPAGO) field campaign was organized (Nesbitt et al. 2021). RELAMPAGO saw the several-month deployment of a wide array of instrumentation throughout the foothills and plains adjacent to the SDC, including the Colorado State University (CSU) C-band Instrument for Hydrological Volumetric Observation (CHIVO) radar, radiosondes, and a NASA lightning mapping array (LMA) through much of the austral warm season, from November 2018 through January 2019.

A key aspect of the design of RELAMPAGO was the intentional co-location of instruments that allow us to directly analyze convective processes vital to storm electrification while simultaneously observing resultant lightning behavior with high quality three-dimensional measurements. CHIVO radar observations combined with frequent and regular radiosonde launches enable detailed hydrometeor identification (HID) analysis, providing the capability to analyze the driving mechanism of charge separation within convective storms; primarily non-inductive charging (NIC) processes (Reynolds et al. 1957, Williams et al. 1991, Saunders et al. 2006). NIC processes occur through rebounding collisions of riming graupel and ice crystals within the mixed-phase region of convective storms (between -5 and -40°C) in the presence of supercooled liquid water. Rebounding collisions between an ice crystal and graupel result in opposite charges on them, where the amount and sign of charge acquired depends primarily on temperature and effective supercooled liquid water content. Under typical conditions within convective storms, NIC processes result in a net negative charge on the graupel and a net positive charge on the ice crystals. The updraft lofts ice crystals to higher portions of the storm while the heavier graupel remains at lower levels. In an idealized storm, this results in a dominant positive charge region in the upper reaches of the storm due to positively charged ice crystals and a negative charge region below the mixed phase region due to negatively charged graupel. In environments with faster and more effective transport of liquid water into the mixed phase region, through strong updrafts and shorter residence time within the warm cloud region, storms may take on an "anomalous" charge structure with negatively charged ice crystals and positively charged graupel, often resulting in flashes occurring lower in the storm (Fuchs and Rutledge 2018). Turbulent updrafts and intra-storm motion complicate these simplified idealized models of charge separation, yet the base physical assumptions stand.

Many past studies have compared kinematic and microphysical storm parameters to lightning flash rates under NIC assumptions, through both spaceborne and ground-based observations. Early work by Petersen et al. (2005) suggested that there is a regionally invariant relationship between TRMM-derived Ice Water Path (IWP) and lightning flash rate, no matter the climatic regime or environment, with observed storms over land, coasts, and the ocean all following similar relationships. Ground-based work from Deierling et al. (2008) and Deierling and Petersen (2008) also found regionally invariant relationships between lightning activity and kinematic and microphysical parameters from a sample of Alabama and Colorado storms. Yet more recent work suggests a more varied relationship, with greater variability in parameterization performance across several US regions and across kinematic and microphysical variables (Basarab et al. 2015, Carey et al. 2019). Most detailed ground-based lightning parameterization work has been done within the US, as it is home to several permanent LMA networks, a robust ground-based radar network, and a long history of detailed field campaign observations. To help address this disproportionate US-bias in coverage, one of RELAMPAGO's key objectives was to provide a similarly robust observational network across the SSA campaign domain to facilitate the creation and comparison of similar regressions and lightning characteristics to those from the US.

Recent work has analyzed the RELAMPAGO dataset to investigate lightning characteristics across the entire spectrum of storms observed during the campaign. Initial results have found lightning parameterizations created from the RELAMPAGO dataset had significant differences when compared to US-based studies, with US-based parameterizations yielding physically unrealistic lightning flash rates when applied to simulations of South American storms

(Rocque 2023, Rocque et al. 2024). Investigation into charge regions within convective storms during RELAMPAGO have found a preference toward the normal polarity structure, with only 13.3% of environments presenting as anomalous, compared to a similar 7.3% anomalous in Alabama and a uniquely dominant 82.6% anomalous in Colorado, observed during the 2012 DC3 field campaign (Barth et al. 2015, Medina et al. 2021). Yet directly comparing parameterizations and lightning polarity behavior across studies and across regions can be challenging, as the many lightning regression studies conducted in the US do not necessarily share a consistent methodology and consistent instrumentation with the RELAMPAGO dataset, having relied on different radars, lightning detection techniques, definitions of what constitutes a "storm" feature, and vastly different sample sizes.

To have confidence in comparing and applying lightning parameterizations across diverse climate regions and campaign datasets, we must aim for a consistent methodology with as similar instrumentation as possible. To that end, after the conclusion of RELAMPAGO in 2019, the CSU-CHIVO radar was returned to its permanent home near Fort Collins, Colorado. Soon after, the Prediction of Rainfall Extremes Campaign in the Pacific (PRECIP), initially planned to deploy to Japan, Taiwan, and Korea during the summer of 2020, was delayed and pushed back to the summer of 2022 due to the COVID-19 pandemic. To take advantage of this two-year pushback, the PRECIP science team conducted the Preparatory Rockies Experiment for the Campaign in the Pacific ("PRE"-CIP) from May through August of 2021. "PRE"-CIP was an opportunity to test experimental design in preparation for the main campaign in 2022, while also collecting a wide range of observations in the semiarid climate of the foothills and plains east of the Rockies in Colorado; a direct contrast to the moist environment of maritime east Asia. During "PRE"-CIP,

the CSU-CHIVO radar was co-located with the permanent Colorado LMA network, which operates with the same technology as the LMA established in Argentina for RELAMPAGO, in addition to soundings launched by the "PRE"-CIP team during periods of enhanced convective activity alongside the regular, 12 hourly (0 and 12 UTC) soundings launched by the National Weather Service (NWS) in Denver, Colorado.

This presents us with a unique and valuable opportunity; two several-month long campaign datasets of nearly continuous observations from co-located radar, radiosondes, and LMAs that capture the entire spectrum of convective and lightning activity across their respective warm seasons, using the exact same radar and similar QC processing techniques for all instruments for both campaigns. Both campaigns targeted convection in the immediate lee of prominent north-south mountain ranges known for driving convective initiation that produces frequent electrically active storms, allowing for observations of several thousand lightning-producing storm features across the warm season of both regions. The consistency in instrumentation and experimental design enables us to avoid some of the most important challenges with previous lightning regression work and allows us to answer our key question; how similar or different are key electrification and lightning characteristics and processes between Colorado and SSA storms when the same instrumentation, similar methodologies, and comparably large sample sizes are used, and how does this compare to previous lightning research? These datasets allow us to conduct the first direct comparison of microphysical drivers to electrification across a spectrum of storm intensities, sizes, and durations between two regions known for intense convection and high lightning flash rates in the immediate lee of prominent mountain ranges.

Chapter 2

METHODS

To answer the key questions and directly compare lightning characteristics between SSA and Colorado for the first time, methodologies developed by Rocque et al. (2024) are applied to both RELAMPAGO and "PRE"-CIP datasets as similarly as possible. Figure 2.1 summarizes the locations of instrumentation used throughout this analysis from both campaigns on topographic maps, plotting the CSU-CHIVO radar, radiosonde launch sites, and the individual stations that comprise each LMA network. The consistency in instrumentation and methodologies applied to both campaign datasets provides greater confidence in producing meaningful direct comparisons across both regions.

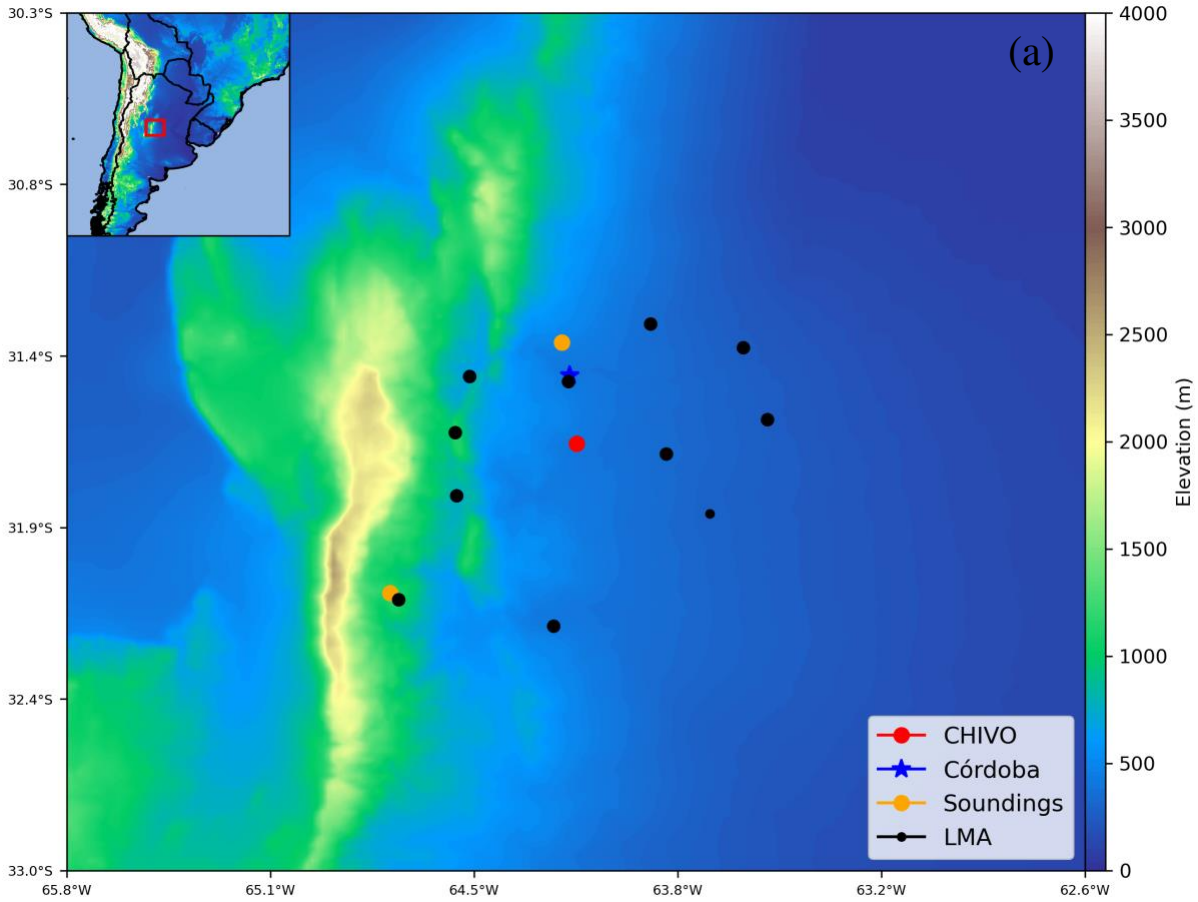

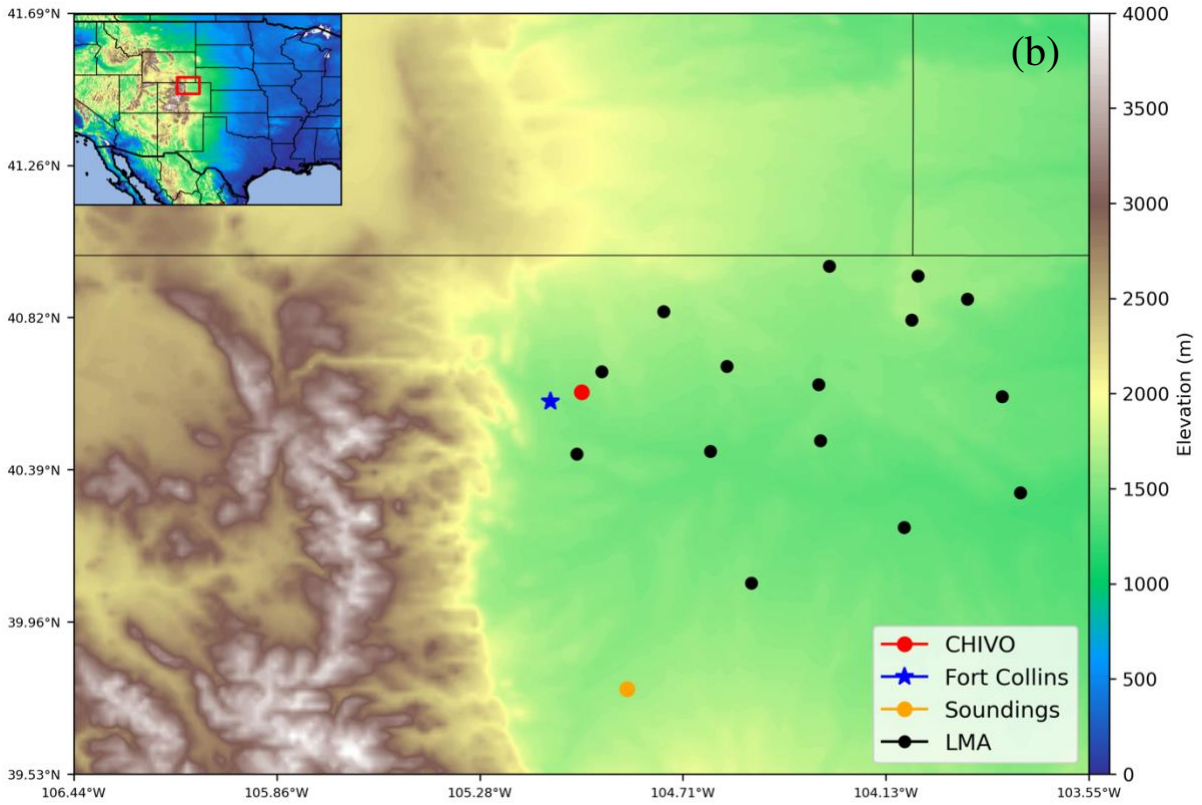

Figure 2.1: Instrumentation summary maps for RELAMPAGO (a) and "PRE"-CIP (b), with topography described by the color shading. Map inlets provide continental context of each campaign's domain. The legend describes the location of the CSU-CHIVO radar (red), LMA stations (black), sounding launch sites (orange), and the nearest major city (blue).

2.1 CHIVO Radar

The Colorado State University C-band Instrument for Hydrological Volumetric Observation (CHIVO) radar was deployed to both regions, allowing for direct comparisons of its observations of precipitation features (PFs) and microphysical characteristics of storms. While scanning strategies differed across campaigns, similar QC procedures and the same hydrometeor-identification (HID) algorithms were used for both datasets, making comparisons across regions as compatible as possible. During RELAMPAGO, CHIVO was deployed 24 km south of Córdoba, Argentina; a city of over 2 million that lies in the immediate lee of the SDC, a secondary range east of the Andes, reaching elevations of up to 9,400' (Arias et al. 2019). CHIVO's location in the

adjacent plains immediately east of the SDC allows for the observation of both the development of convection over the terrain as well as the propagation of this convection east over the plains, providing continuous observations across a storm's evolution and potential upscale growth. CHIVO performed a predetermined 10-minute scan cycle with the ability for a user to modify portions of the routine during periods of enhanced convective activity for more directed and focused observations. A typical scan routine consisted of a combination of both 360° plan position indicators (PPIs) and range height indicators (RHIs), with a typical PPI cycle made up of 20 elevation angles from 0.5 to 19°, with the option to add a 135° sector scan (SEC) focused over the terrain during periods of active development. These SEC scans were only chosen when storms over the terrain were active and the rest of the domain was comparatively quiet. CHIVO's beam is partially blocked to its west from 240-300° azimuth by the SDC at its lowest elevation angles between 1-1.5° (Nesbitt et al. 2021 and Rocque et al. 2024).

During "PRE"-CIP, CHIVO scanned from its permanent home 3 miles northeast of Fort Collins, Colorado, a city of 170,000 in the immediate lee of the Rockies. Similar to the strategy employed in Argentina, this location allows the radar to observe storm initiation over the Rockies and foothills to the west as well as storm evolution as they propagate east over the plains. CHIVO performed a predetermined 12-minute scan cycle of PPIs and RHIs, with 12 PPI elevation angles from 0.5 to 15°. As in RELAMPAGO, a user could have the ability to modify certain portions of the routine during periods of enhanced convective activity. Both campaign datasets underwent similar QC processing, using methods developed by Rocque et al. (2022) to correct for biases, non-meteorological echoes, attenuation, and clutter, often from the terrain (Vivekanandan et al. 1999, Dolan et al. 2013). Next, both sets of radar data were interpolated to a 1 km horizontal

resolution and 0.5 km vertical resolution grid using the LROSE package's Radx2Grid application (LROSE, Bell et al. 2022). The Dolan et al. (2013) Hydrometeor Identification (HID) algorithm was applied to this gridded CHIVO data to group radar returns into 10 hydrometeor categories. Due to our interests in NIC processes and storm electrification, we group these 10 categories into more broad classifications of either graupel, hail, snow, or ice. The nearest sounding to each radar scan, as described in section 2.2, is used to identify the freezing level and temperature profile, which are necessary for the HID algorithm to determine particle phase and type. After categorization into hydrometeor type, Z-M relationships are applied to quantify the mass of each hydrometeor within a grid box. To remain consistent across a broad range of previous lightning regression work, the Z-M relationships defined by Heymsfield and Palmer (1996) and Heymsfield and Miller (1998) are used for hail, graupel, and snow/ice (Deierling et al. 2008, Basarab et al. 2015, Carey et al. 2019).

2.2 Soundings

Soundings were launched from 15 mobile and permanent platforms during RELAMPAGO, yet for this analysis we focus on two sites; the M1:Córdoba ARM instrumentation site and the Córdoba Airport (Nesbitt et al. 2021, Schumacher et al. 2021). Soundings were launched regularly from the M1:Córdoba ARM instrumentation site, located 94 km southwest of Córdoba at 1122 m elevation ASL, and are used in this analysis to identify the environmental freezing level and temperature profile; crucial for the HID algorithm described in Section 2.1. These soundings occur several times each day for the entire duration of the campaign, with regular launches at 00, 12, 15, 18, and occasionally 21 UTC, meaning we have temperature profile information for any CHIVO scan within a reasonable temporal range. However, because these soundings were launched from

a relatively high elevation amidst the terrain of the SDC, mountain fog and developing storms often form near the instrumentation site, leading to frequent instances of low-level saturation in the sounding data. This makes the potential calculation of low-level metrics such as lifting condensation level (LCL) and warm cloud depth (WCD) challenging. Despite these challenges in low level saturation, this does not dramatically impact a sounding's ability to capture the temperature profile above freezing, meaning we can continue to confidently use these soundings for HID calculations, as has been done in previous work during RELAMPAGO (Rocque et al. 2024).

To calculate LCL and WCD, lower-elevation soundings launched from the Córdoba Airport (473 m ASL) are used. These low-elevation soundings don't match the high frequency of the M1:Córdoba ARM site, yet most days still saw at least two launches, with a higher frequency during periods of active convection. Any sounding with an LCL lower than 200 m AGL is removed from the dataset to avoid convective contamination influences on LCL and WCD statistics. Due to this decrease in launch frequency and removal of contaminated soundings, simply finding the temporally nearest sounding to each radar scan would potentially result in atmospheric profiles being attributed to radar scans that occurred up to two days apart. This would be clearly unrepresentative, so a 12-hour maximum temporal difference filter is applied, meaning that if there is no sounding 12 hours before or after a given radar scan, no low elevation sounding is paired and no LCL or WCD calculations are done. Because of the consistently high frequency of the higher elevation M1:Cordoba soundings, this 12-hour maximum temporal difference filter is very rarely applied, meaning we have HID and freezing level measurements for nearly all radar scans, as the HID relies solely on these frequent high elevation soundings. Yet LCL and WCD calculations,

which solely rely on the low elevation soundings that have less low-level contamination, do not cover all radar scans and all storm features. The number of radar scans that have a low-level sounding within the +/- 12-hour window is still large enough to perform meaningful statistics, but it must be noted that this does not represent complete coverage of the campaign throughout January.

Soundings launched throughout "PRE"-CIP came from only two sources; regular, twice daily (0 and 12 UTC) soundings launched in Denver by NWS Boulder and those launched by the "PRE"-CIP team in northern Colorado during periods of active convection. While the campaign-launched soundings were often spatially very close to the target convection, they were not temporally consistent, as they were only launched when the investigators deemed it necessary. The physically more distant (90 km) yet temporally consistent Denver soundings act to fill in gaps during times when there may have been weak convection within the domain, yet not strong enough to warrant a manual campaign launch. Filling in these gaps in sounding availability is crucial, as a key objective of this study is to examine the entire spectrum of electrified storms; even weaker storms with low flash rates. The same 12-hour temporal filter from RELAMPAGO is applied to the "PRE"-CIP soundings, but due to the consistent 0 and 12 UTC Denver launches, supplemented by the campaign-launched soundings, there is no instance where the 12-hour filter becomes relevant. There is always a sounding within 12 hours of each radar scan, meaning HID, LCL, and WCD calculations are possible for every storm feature observed by CHIVO across the entire campaign.

2.3 Feature Identification

To directly compare radar-derived storm features with lightning behavior, we must define what exactly constitutes a "storm feature". Through use of an algorithm developed by Rocque et al. (2024), modified from the Rocque and Rutledge (2021) algorithm, regions of continuous >0 dBZ echo between 3-5 km above radar level are defined as a Precipitation Feature (PF), of which an ellipse is drawn around to define its horizontal extent. By identifying features using composite reflectivity from 3-5 km, we ensure that we capture precipitating events that have the potential for ice processes and electrification; not liquid cloud-only features that are less relevant for lightning. Convective/stratiform partitioning is done by the Steiner et al. (1995) algorithm, finding ellipses within an already defined PF that encapsulates contiguous regions of convective or stratiform pixels. By definition, a convective or stratiform feature is a subset of a PF; there cannot be one without a parent PF of contiguous 0 dBZ echo. A final level of partitioning is done to investigate the most intense cases of both convective and stratiform features, motivated by the Houze et al. (2015) analysis of 16 years of TRMM Precipitation Radar (PR) observations. These "storm mode" partitions are extreme subsections of the initial convective/stratiform Steiner-defined features; exceptionally tall, wide, and/or intense convective storms and exceptionally broad stratiform features. Storm modes consist of deep convective cores (DCC), wide convective cores (WCC), deep and wind convective cores (DWCC), and broad stratiform regions (BSR). Each storm mode feature must meet certain reflectivity with height or width thresholds to be classified, shown in Table 2.1. A DWCC feature is defined as a convective core meeting both the DCC and WCC thresholds.

Table 2.1: Reflectivity and echo top height threshold differences for TRMM-heritage storm mode classifications between Rocque et al. (2024) and this study.

Rocque et al. 2024	This study
DCC: 40 dBZ >10km	**DCC**: 35 dBZ > 9km
WCC: 40 dBZ > 1,000 km^2	**WCC**: 35 dBZ > 900 km^2
BSR: >10,000 km^2	**BSR**: >10,000 km^2

Slightly modified reflectivity and echo height thresholds were used in this work than in Rocque et al. (2024), which followed the Houze et al. (2015) "strong" thresholds for feature identification. In our study, we split the difference between the "strong" and "moderate" threshold, defining the "deep" threshold as 9 km and the convective threshold as 35 dBZ, which captures a more relevant portion of the storm for lightning than the "strong" 10 km and 40 dBZ thresholds. The area threshold for broad stratiform regions was lowered from the original 50,000 km2 to 10,000 km2 in Rocque et al. (2024) due to the CHIVO domain size; a change we maintain in our study. These changes ensure that our thresholds aren't prohibitively strict, and that a meaningful sample size can be gathered in both regions. For all PFs, convective/stratiform features, and storm modes, a suite of variables were calculated to facilitate comparison across features and across campaigns. The 2D footprint area of each feature, the echo top height of relevant reflectivity values, and radar HID-derived volumes of key microphysical parameters are all calculated. All thresholds used and decisions made for feature identification are identical for both campaigns. Additionally, the 35 dBZ echo volume for each feature was calculated. This volume is a commonly used proxy for lightning, as it captures much of the key processes necessary for NIC yet requires no HID calculations as it is found directly from the radar returns.

2.4 Lightning Mapping Array

To detect lightning flashes associated with radar-observed storm features, both campaigns collected data from ground-based Lightning Mapping Arrays (LMA) (Rison et al. 1999). While Colorado is home to a permanent LMA network in the lee of the Rockies consisting of 15 ground-based stations used during "PRE"-CIP, a NASA LMA was temporarily installed in Argentina during RELAMPAGO, with 11 stations co-located with CHIVO in the lee of the SDC (Lang et al. 2020). Where spaceborne optical lightning sensors such as GLM may struggle with detecting low level flashes due to attenuation through thick clouds, ground-based LMAs are able to capture nearly all flashes throughout their network range (Rutledge et al. 2020). Very high frequency (VHF) emissions from lightning breakdown processes are emitted isotropically, allowing all active sensors within an LMA network to detect these VHF "sources", yet at slightly different times. Time-of-arrival techniques are used to estimate where in space and time these VHF sources likely occurred, allowing for the 3D mapping of most lightning flashes within the LMA domain within 100 km of the network center (Proctor 1971, Chmielewski and Bruning 2016). In both regions, sources are grouped into discrete lightning flashes if they occur within 150 ms or 3 km of each other, with a maximum total flash duration of 3 s, achieved by the lmatools software from Bruning et al. (2014). For time-of-arrival algorithms to be accurate in mapping flashes in three dimensions, at least 6 stations were required to be active for both LMA networks. The RELAMPAGO LMA was exposed to more background VHF noise than the Colorado LMA, meaning it required a more lenient chi-squared goodness of fit requirement of 5.0, compared to 2.0 for Colorado (Deierling et al. 2008, Lang et al. 2020). Beyond simply counting lightning flashes, the LMA measures the area, height, duration, and energy of each individual flash, which is accumulated and output over ten-minute periods. Figure 2.1 shows the locations of all LMA stations within both the Colorado LMA

network as well as the network established for RELAMPAGO. Both networks cover the plains east of their relevant terrain, co-located with CHIVO, allowing for continuous lightning observations throughout the convective life cycle of most relevant storms.

2.5 Lightning Regressions

To relate CHIVO-observed microphysical characteristics of discrete storm features defined in section 2.3 to lightning behavior, each individual LMA output file is matched to the temporally nearest CHIVO file, whether before or after. Once an LMA file is paired with a CHIVO file, it must then be determined whether each discrete flash can be attributed to a discrete storm feature. Each VHF source point that makes up a given flash is used to find the geographic center, or "centroid", of the flash. The location of the centroid is then compared to the 3-D volumes of available PFs, convective/stratiform features, or TRMM-heritage storm mode features present in the paired CHIVO file for that time. If the centroid lies within the volume of one of these features, that flash is now attributed to it and paired. This process is repeated for every flash across every 10-minute LMA file, yielding 620,550 valid and paired flashes in Colorado and 821,951 in SSA. A flash can be attributed to multiple storm features, given that the smaller feature, such as a TRMM-heritage storm mode, is contained within a parent PF or convective/stratiform feature. If a flash's centroid is not co-located with any radar feature, that flash is not used for any future statistics or comparisons. Flash rates are calculated across the duration of a full CHIVO scan by dividing the number of paired flashes by the duration of the CHIVO scan, as was done in Rocque et al. (2024). Linear regressions are created between radar-derived microphysical / storm-intensity parameters and lightning flash rate, allowing for a direct comparison across the two campaigns in how charging processes may or may not differ and how resultant lightning may respond. While

past work has had success in relating lightning flash rates to kinematic variables such as updraft speed and upward flux (Deierling et al. 2008), dual-doppler analysis was beyond the scope of this analysis. Regressions are forced through zero to remove non-physical negative flash rates or microphysical parameters that would interfere with our interpretation of their conclusions, as is done in most lightning regression studies (Basarab et al. 2015, Carey et al. 2019, Rocque et al. 2024).

CHAPTER 3

RESULTS

Results are presented that compare topographical and microphysical drivers to convection and electrification between both campaign datasets. Consistency in instrumentation and methodologies allow us to make the first direct and systematic comparison of electrification processes between these regions.

3.1 Storm Characteristics and Associated Lightning

Table 3.1: Total count of CHIVO-observed precipitation features, convective / stratiform features, and TRMM-heritage storm modes with co-located lightning from both campaigns.

	RELAMPAGO	"PRE"-CIP
PF	2767	4024
Convective	8195	7317
Stratiform	3339	3920
DCC	3298	3286
DWCC	279	1
BSR	734	273

Table 3.1 summarizes the PF, convective and stratiform features, and TRMM-heritage storm mode counts from each campaign. Recall that thresholds used to define each feature type were identical across both campaigns using the same ground-based radar, allowing for confidence in the consistency of any direct comparisons. The only major difference that may add uncertainty in direct comparison is the length of the observational period. During RELAMPAGO, CHIVO ran

from 11/10/18 through 1/31/19 (82 days), with breaks in observations during convectively inactive periods or during maintenance. During "PRE"-CIP, CHIVO ran from 5/1/21 through 8/31/21 (122 days), again with breaks during inactivity or maintenance. Yet despite the longer observational period of "PRE"-CIP and ~45% more PFs observed as a result, SSA still produced more convective features, DWCCs, and BSRs. Both campaigns recorded nearly identical counts of DCC features, yet far more DWCCs were observed in SSA than in Colorado. While both regions are home to favorable environments for convective initiation and generally deep storms, the SDC in SSA is home to frequent back-building, allowing for convection to grow horizontally and upscale, while Colorado storms remain more isolated as they often translate quickly to the east. Similarly, SSA saw nearly three times as many BSR features than Colorado, likely due to large trailing stratiform regions formed behind eastward-propagating MCSs, which isolated DCC features would not develop or support. Figure 3.1 examines the distribution of PF and storm feature areas, finding systematically larger PFs in SSA than in Colorado, which agrees with the back-building framework for convection in SSA.

Satellite radar climatologies from the TRMM satellite showed that SSA has among the deepest convective storms on Earth (Zipser et al. 2006; Houze et al. 2015). Numerous studies have examined the nature of convective storms in SSA (Nesbit et al. 2021; Rasmussen and Houze 2011, 2016; Mulholland et al. 2018), their seasonality (Romatschke and Houze 2010; Rasmussen et al. 2016), and connections to large-scale synoptic features (Bruick et al. 2019; Piersante et al. 2022). However, this study provides an unprecedented opportunity to directly compare RELAMPAGO and "PRE"-CIP radar observations using the same ground-based radar system. Figure 3.2 shows distributions of 20 and 35 dBZ echo top heights and clearly demonstrates that SSA features are

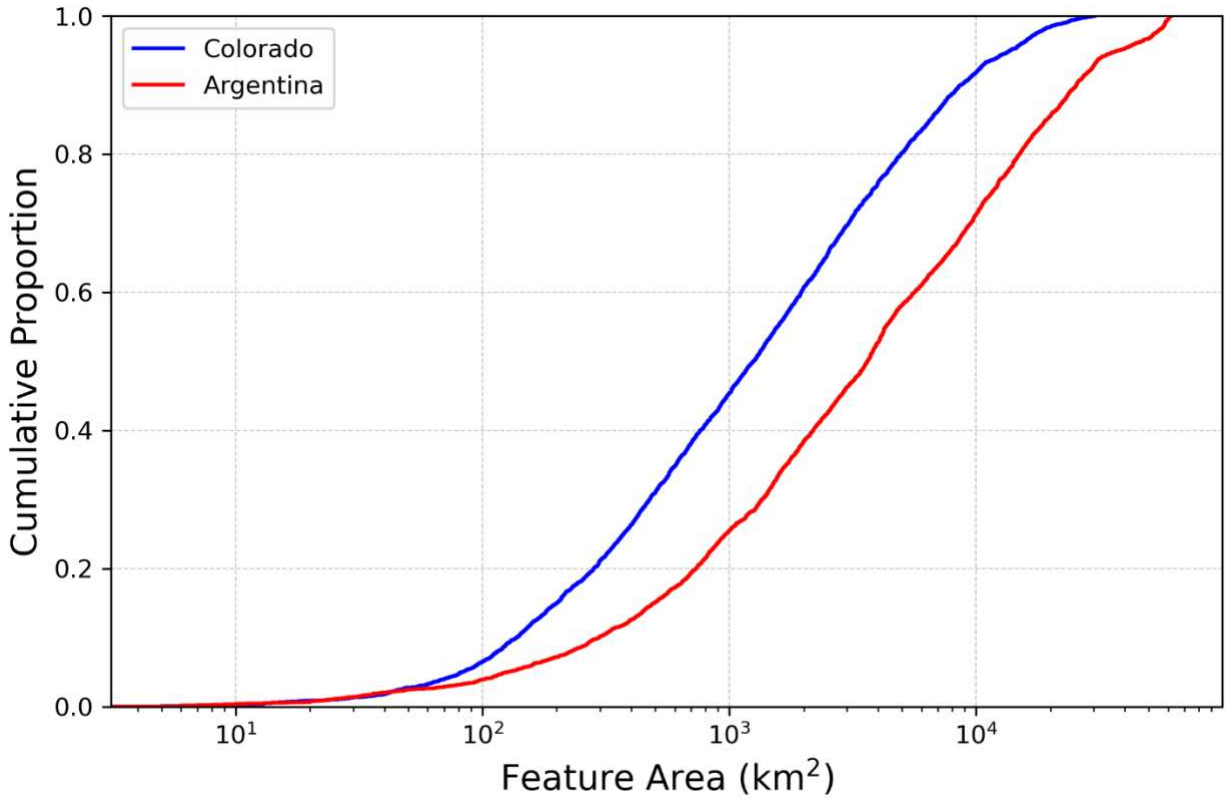

Figure 3.1: Cumulative distribution plot of radar-defined precipitation feature (PF) areas (km^2) for RELAMPAGO (red) and "PRE"-CIP (blue).

systematically more intense and deeper than those in Colorado. The 35 dBZ echo threshold is considered a useful proxy for identifying the core of the most intense convective activity within a storm as well as lightning processes (Liu et al. 2012), while the 20 dBZ echo is useful to capture relative differences in echo top heights closer to the top of the storm. Figure 3.2 highlights a crucial difference seen in the distribution of the 35 dBZ echoes, with a tail of exceptionally tall echo tops in SSA, consistent with spaceborne studies of the intensity of Argentinian convection in comparison to other convectively-active regions (Zipser et al. 2006; Houze et al. 2015).

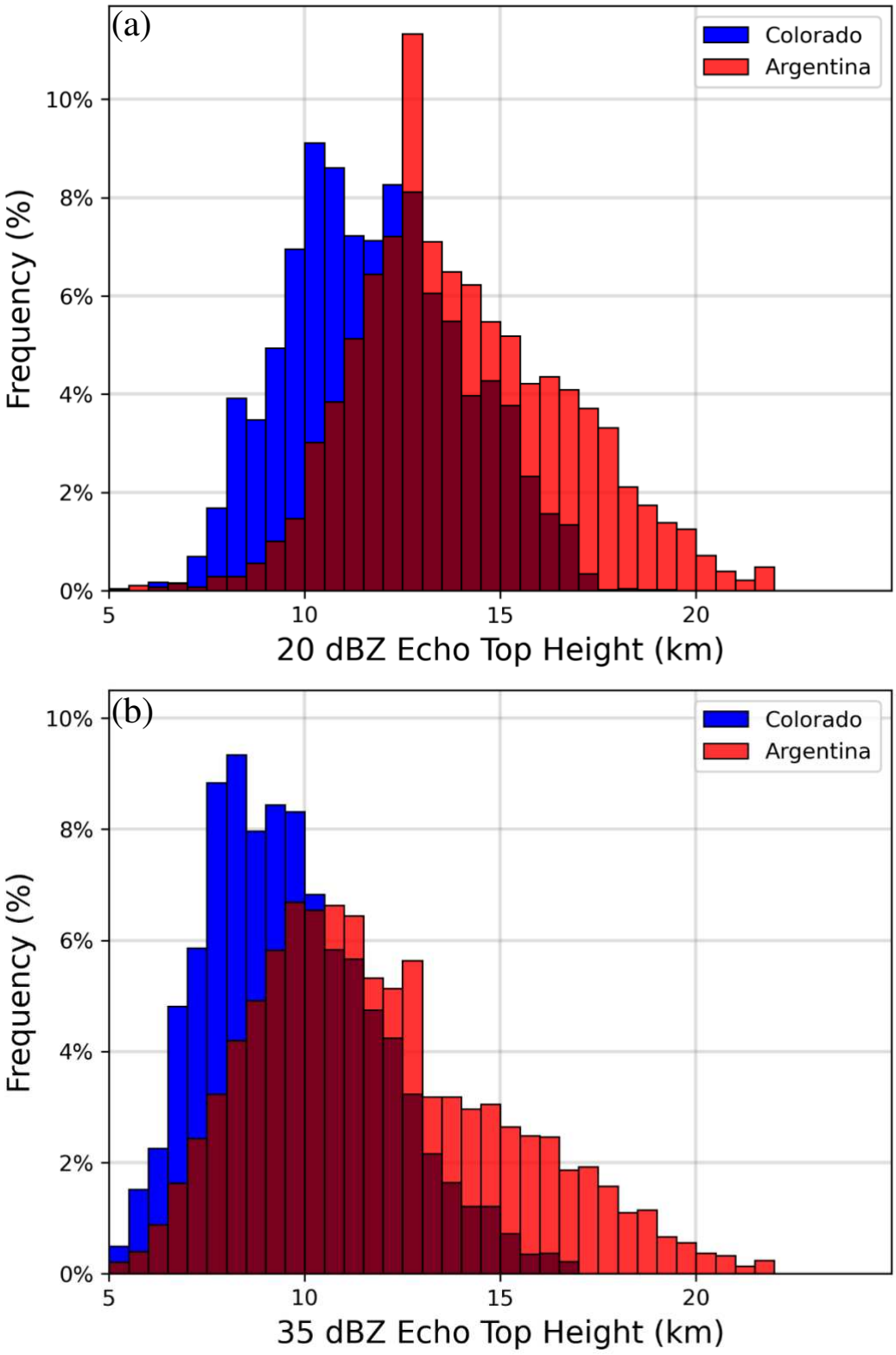

Figure 3.2: Histograms of the 20 dBZ (a) and 35 dBZ (b) echo top heights (km AGL) for every PF identified from RELAMPAGO (red) and "PRE"-CIP (blue) that had co-located lightning present.

The combined results from Figures 3.1 and 3.2 show that PFs in SSA are generally taller and larger in area compared to those in Colorado and likely indicates frequent upscale growth processes tied to the SDC, allowing storms time to back-build and develop upscale before moving east over the plains (Romatschke and Houze 2010; Rasmussen and Houze 2011, 2016). Colorado storms initiate over the mountains and move eastward over the plains as more discrete convection far more quickly (Carbone et al. 2002, Douglas 2024), providing less time to grow upscale and intensify in the direct vicinity of the foothills of the Rocky Mountains, hence the lack of identified DWCCs seen in Table 3.1. The taller Andes produce a stronger capping inversion and higher CAPE and CIN than shorter simulated mountain heights, allowing for more intense and explosive convection initiation than is likely possible downwind of the shorter Rockies (Rasmussen and Houze 2016).

A close examination of the location of every flash observed by the LMA that was paired to a PF across each full campaign is shown in Figure 3.3. It is immediately clear that flashes over the RELAMPAGO domain preferentially occur over the SDC terrain while flashes over the "PRE"-CIP domain occur overwhelmingly over the adjacent plains east of the Rockies. This agrees with the discussions from the previous figures, as well as previous work done by Rasmussen et al. (2014), which through use of the TRMM satellite's Lightning Imaging Sensor (LIS) found that flashes occur more frequently and often exhibit back-building characteristics over the SDC. In addition, modeling studies over SSA highlight the importance of the Andes and the SDC in promoting upscale growth, and that in simulations with reduced terrain, convection is weaker, produces less lightning, and occurs further east over the plains; similar to what we see in

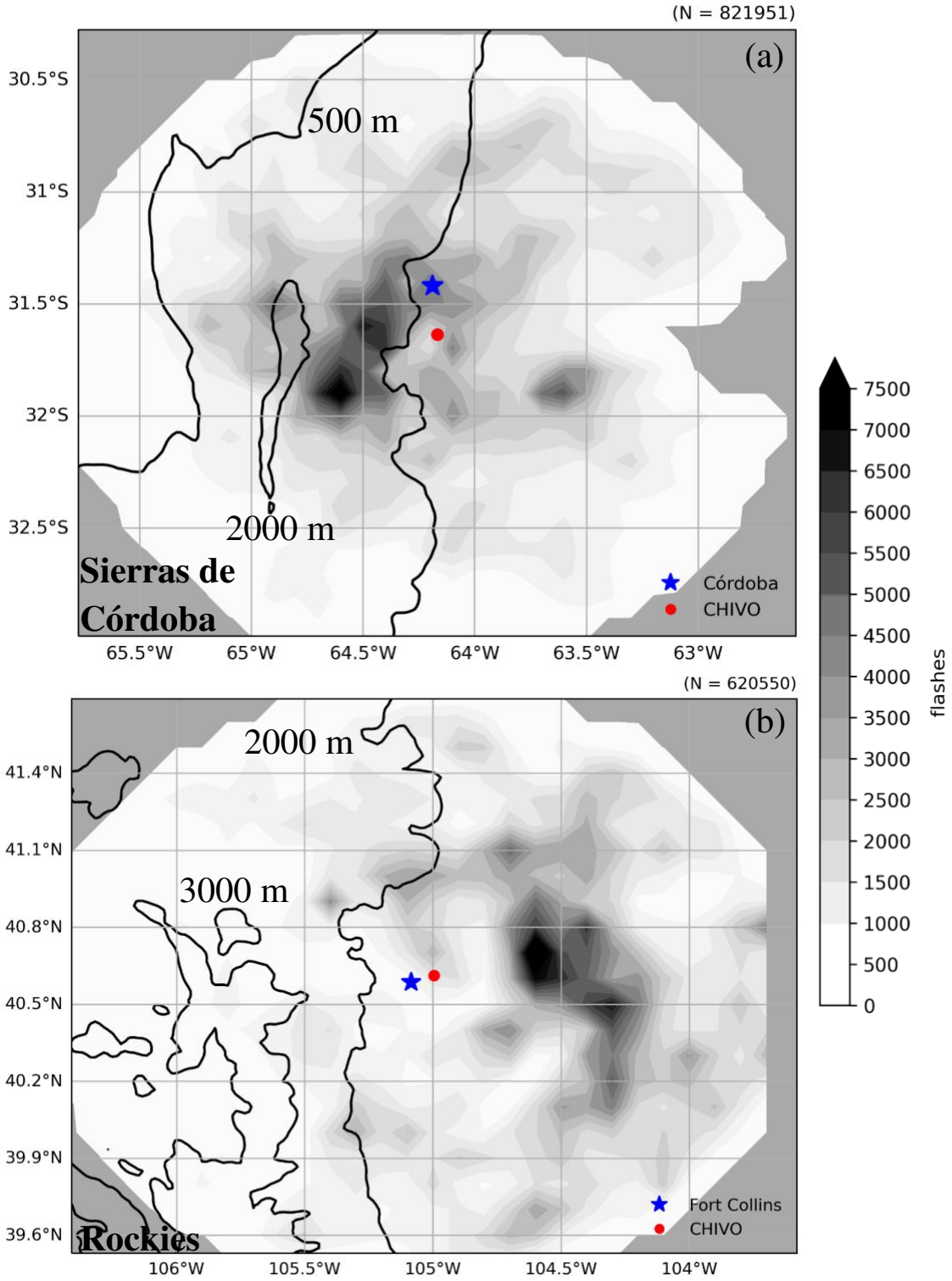

Figure 3.3: LMA-observed lightning flashes attributed to PFs for both the RELAMPAGO domain (a) and the "PRE"-CIP domain (b) on topographic maps, with the location of CHIVO and the nearest major city depicted by the red circle and blue stars respectively. Contours represent 500 m and 2000 m elevation for Sierras de Córdoba (a) and 2000 m and 3000 m elevation for the higher altitude Rockies (b).

observations from “PRE”-CIP in Colorado (Rasmussen and Houze 2016, Rocque and Rasmussen 2022). A preference for larger PFs with more embedded convective features, higher echo top heights, and increased lightning activity linked to the terrain suggests significant differences in storm development and electrification between SSA and Colorado. In SSA, terrain-induced upscale growth leads to broader, more intense storms that dominate the region, in contrast to the more diffuse and plains-oriented storm patterns observed in Colorado.

3.2 Lightning and Microphysics Regressions

Next, an examination of detailed individual storm characteristics is conducted to investigate how differences in microphysical drivers of electrification through NIC processes manifest through flash rate regression comparisons. The relationships between LMA-observed lightning flash rates and CHIVO-observed microphysical parameters are explored through creating campaign-wide scatter plots that allow us to visualize and quantify how a given parameter is related to lightning activity. We use methods developed by Rocque et al. (2024) to complete this analysis, with the key addition of a direct comparison across campaign datasets.

Figure 3.4 consists of four scatter plots comparing LMA lightning flash rates and radar-derived lightning-relevant variables for SSA and Colorado. Each scatter plot follows the same structure, with each individual point representing a single PF that had at least one co-located flash within its volume, with color shading representing the total echo top height of that specific PF. Axes are logarithmic to capture the wide range of 35 dBZ volume, graupel volume, graupel mass, IWP, and lightning flash rates across the broad spectrum of storms in both campaign datasets. As shown in Table 3.1, there were 2767 PFs observed during RELAMPAGO and 4024 PFs observed during “PRE”-CIP that had co-located lightning. Linear regressions are shown for each campaign

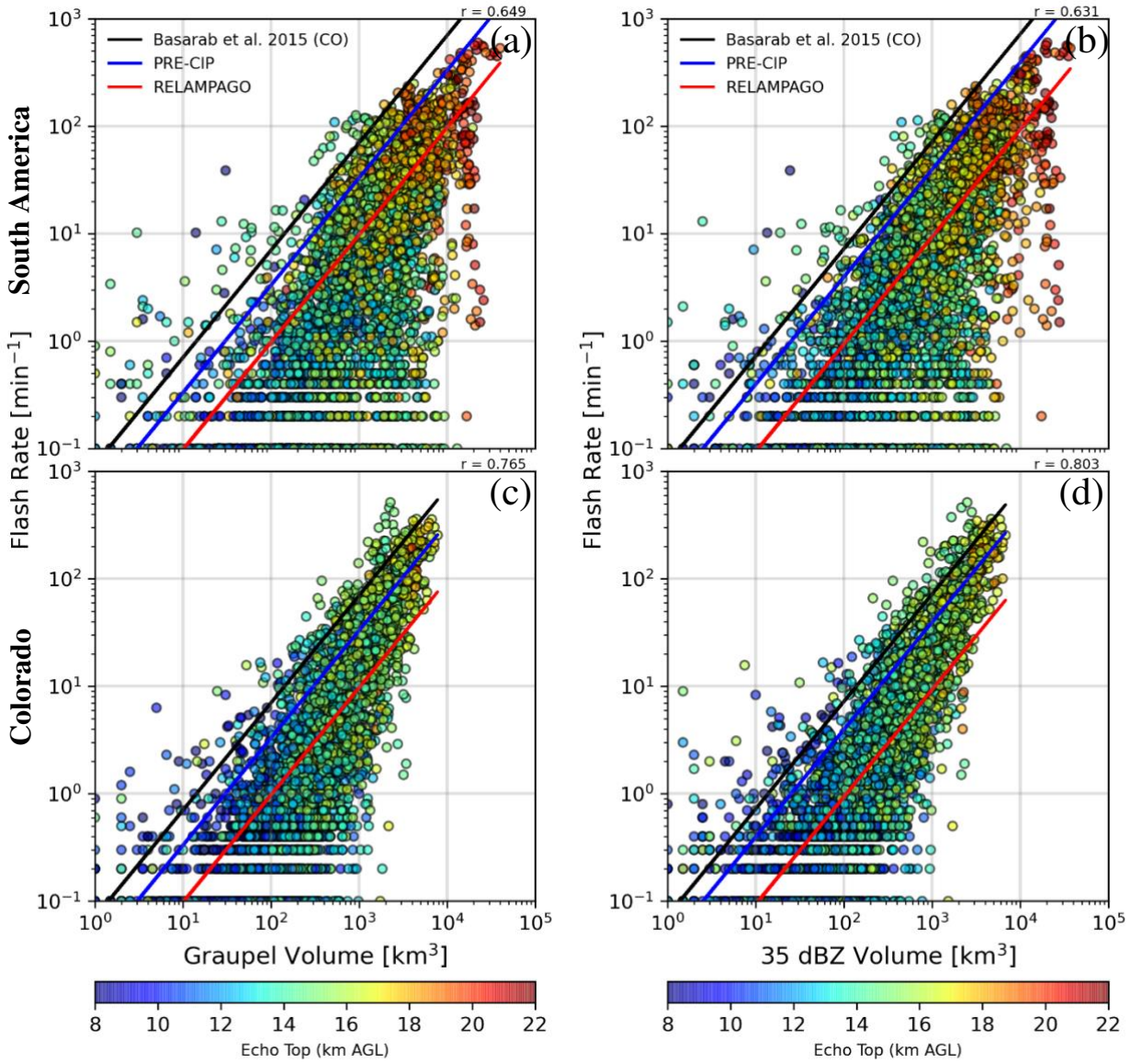

Figure 3.4: Scatter plots of lightning flash rates (min^{-1}) vs. total graupel volume (km^3) (a, c) and total 35 dBZ volume (km^3) (c, d) for all PFs with lightning flashes across both campaigns, with logarithmic axes and color shading depicting echo top height (km AGL). The first row (a-b) are the observations from RELAMPAGO for each variable while the second (c-d) displays "PRE"-CIP. Linear regressions are shown for RELAMPAGO (red) and "PRE"-CIP (blue) datasets for each variable, with the correlation coefficient (r) of the relevant linear regression displayed at the top right of each plot. The Basarab et al. (2015) regression for both variables are shown in black for comparison.

dataset in red (RELAMPAGO) and blue ("PRE"-CIP"), with the addition of the Basarab et al. (2015) regression from their 11-storm study in Colorado. Regressions are forced through zero to ensure there are no non-physical negative predicted flash rates.

Recall from the Introduction that 35 dBZ volume is a commonly used radar proxy for regions of effective electrification within a convective storm. This region encapsulates most of where NIC processes likely occur, with rebounding collisions between graupel and ice crystals within the mixed phase region. PFs observed over SSA reach far greater 35 dBZ and graupel volumes and have systematically higher echo top heights compared to those in Colorado (Fig. 3.4). While the regression created from the "PRE"-CIP dataset (blue line) does not exactly match the Basarab et al. (2015) regression from their Colorado work (black line), they are significantly closer together than the RELAMPAGO regression (red line), which has a considerably less steep slope than both from Colorado (recall the logarithmic axes). Additionally, the SSA dataset has greater spread in its flash rates and microphysical parameters than the Colorado dataset, including PFs that frequently reach echo tops higher than Colorado PFs, with the greatest volumes of 35 dBZ and graupel seen across both campaigns, resulting in the stronger correlations found in Colorado. It is reassuring to find similar correlations for both 35 dBZ volume and graupel volume within each region, as both are intended to capture similar portions of the PF crucial for NIC processes. Due to its similar performance to graupel volume, and that the 35 dBZ parameter requires no HID calculation, 35 dBZ is further examined in place of graupel volume throughout the rest of this study.

Similar to Figure 3.4, Figure 3.5 follows the same structure of plotting scatterplots of all electrically active PFs from both campaigns, but for graupel mass and IWP. IWP represents the sum of all ice hydrometeors within a storm feature, capturing ice both directly and indirectly involved in NIC processes. Again, a similar pattern of the more shallow and less steep RELAMPAGO regressions than "PRE"-CIP regressions for both variables is seen, with a greater

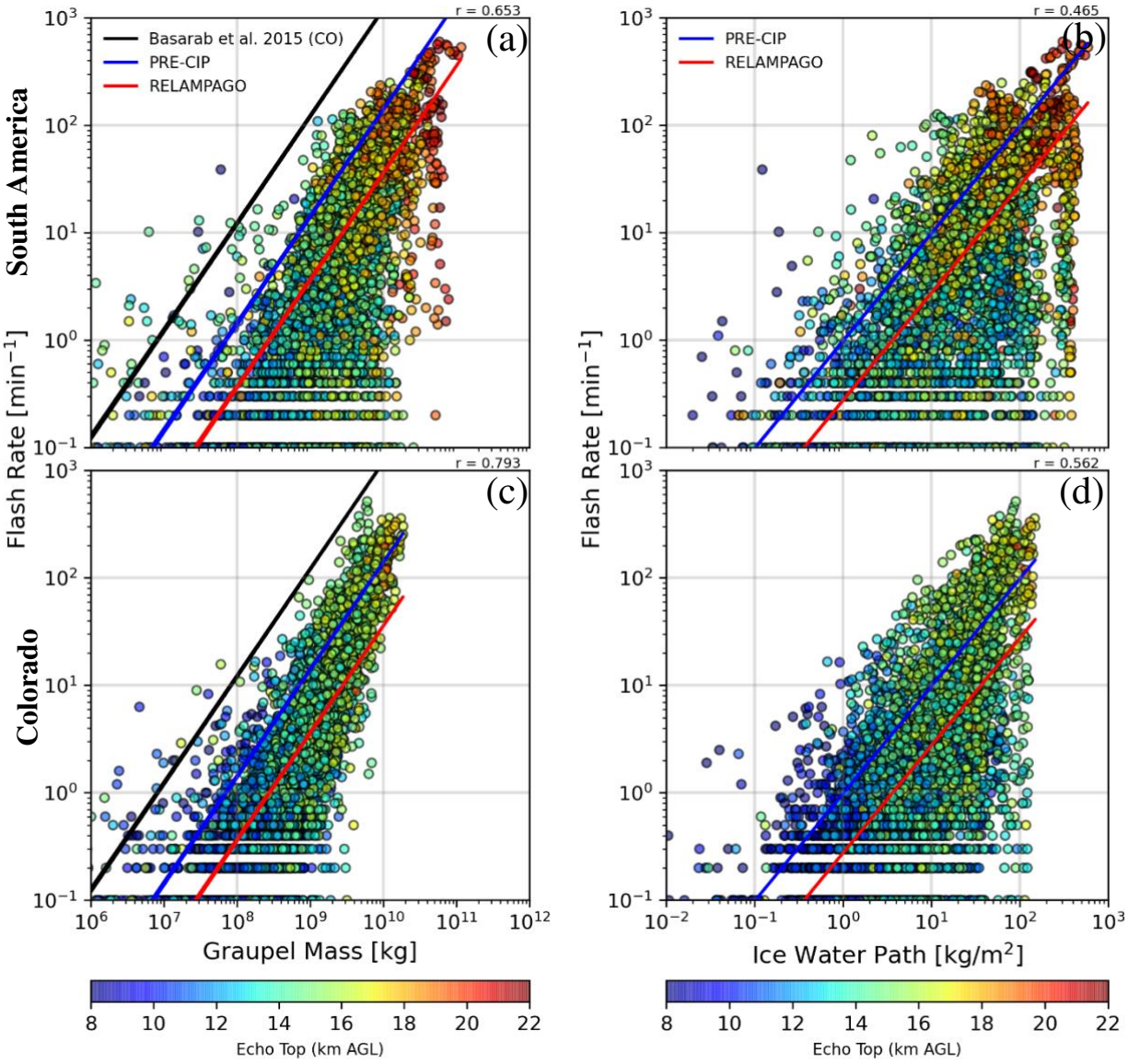

Figure 3.5: As in Fig. 3.4, but for graupel mass (kg) (a, c) and ice water path (kg / m^2) (b, d).

spread in observed graupel mass and IWP throughout the SSA samples. While Basarab et al. (2015) did not calculate IWP for their 11 Colorado storm features, comparisons to their graupel mass regression shows greater differences to our Colorado-based graupel mass regression, yet both are still far offset from SSA. The greater differences in the two Colorado regressions could be a result of our large sample size capturing a more comprehensive picture of the spectrum of electrically active storms over three months, or differences in instrumentation and data analysis

techniques. As seen previously for graupel volume and 35 dBZ volume, the SSA regressions have lower r values compared to those from Colorado for both graupel mass and IWP, yet IWP has the weakest correlation in both regions.

Regression scatter plots built from logarithmic axes may be challenging to interpret by eye, with data at larger values being disproportionately easier to distinguish. An alternate visualization using Kernel Density Estimate (KDE) plots is shown in Figure 3.6, with linear axes for 35 dBZ volume, graupel mass, and IWP. Due to the linear axes used in KDE plots, it is immediately clear how much greater the spread is for all key microphysical variables as well as lightning flash rates from SSA than in Colorado. Additionally, linear axes help display just how extreme the regressions for SSA are compared to all three US-based regressions. While the regressions calculated in this study for "PRE"-CIP PFs still have significant differences to these previously-made US regressions, as potentially expected by the large sample size differences across studies, the RELAMPAGO regressions stand out as consistently and systematically less steep. No matter the variable, SSA storms appear to require significantly greater amounts of all key microphysical parameters to produce an equivalent flash rate compared to storms in Colorado. Like Rocque (2022), we find a significant overestimation of predicted lighting flash rates when our US-based regression is applied to radar observations from Argentina, demonstrating region-wide characteristic differences in electrification efficiency.

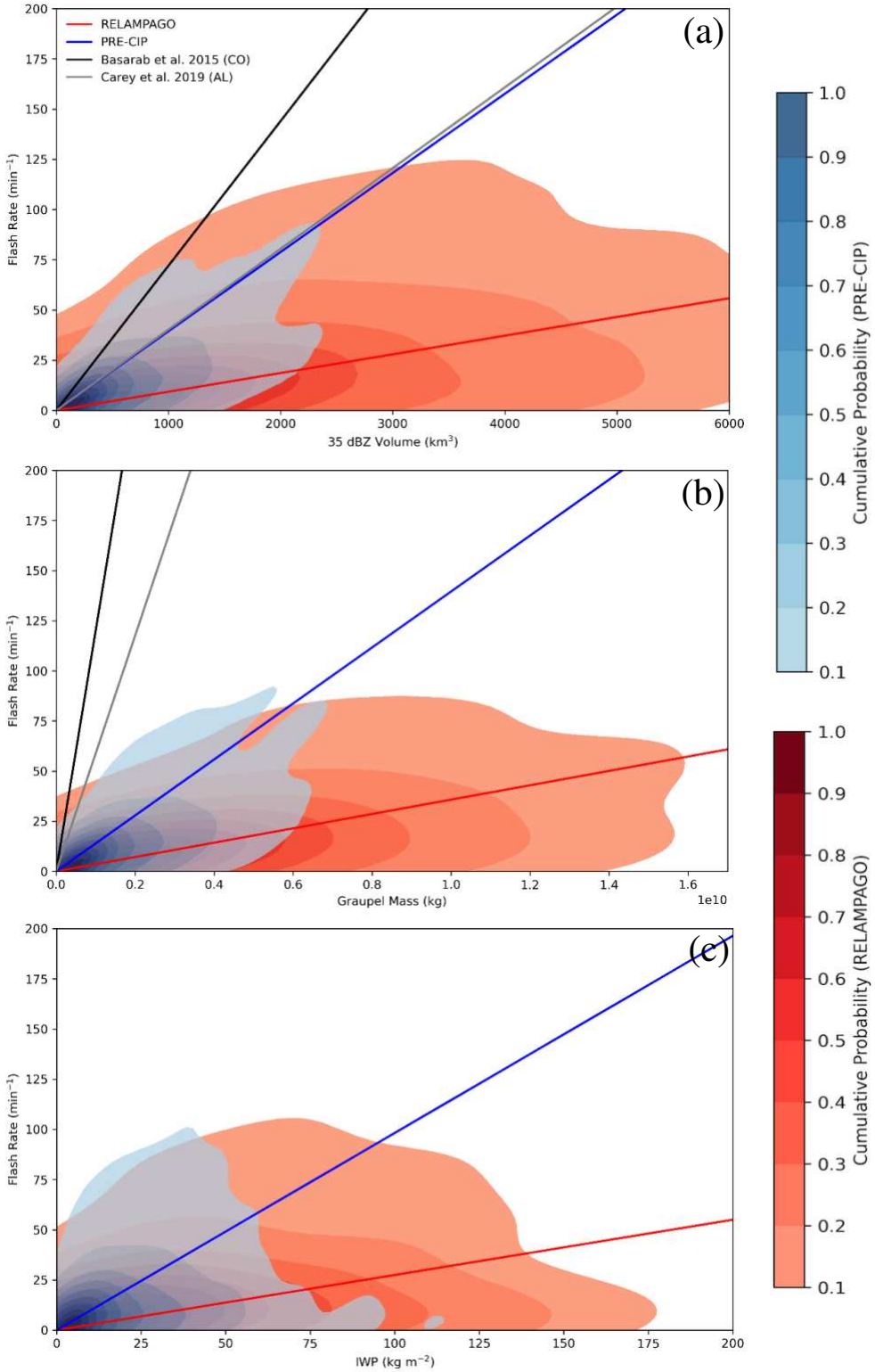

Figure 3.6: Kernel density estimate plots for 35 dBZ volume (kg/m^3) (a), graupel mass (kg) (b), and IWP (kg m^{-2}) (c) for both RELAMPAGO (blue) and "PRE"-CIP (red), on linear axes. Shading represents the probability of data falling within each contour, relative to the absolute maximum probability (1.0). Linear regressions calculated in Figs. 3.4-3.5 are shown in solid red and blue lines. The Basarab et al. (2015) and Carey et al. (2019) regressions are shown in black and gray for 35 dBZ volume (a) and graupel mass (b).

3.3 Convective/Stratiform Regressions

While scatterplots and KDEs of PFs reveal climatological differences in electrification processes and resulting lightning across all PFs (Figs. 3.4-3.6), they provide limited insight into the distinction between convective and stratiform features and how each may respond differently to electrification processes. Lightning flash regressions for convective and stratiform PFs identified by the Steiner et al. (1995) separation algorithm are shown in Figures 3.7-3.8.

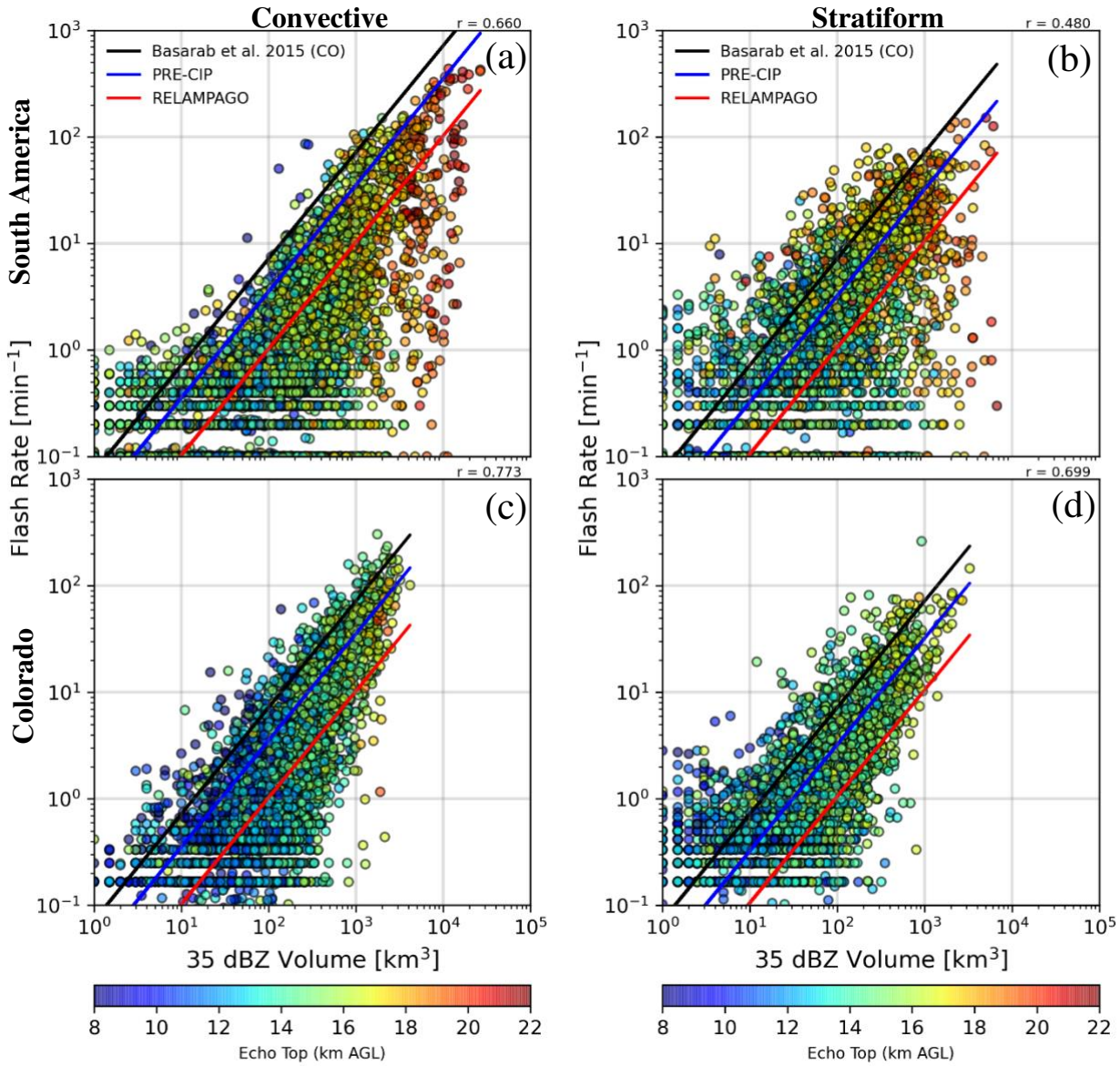

Figure 3.7: As in Figs. (3.4-3.5) except panels are scatter plots of lightning flash rates (min^{-1}) vs. total 35 dBZ volume (km^3), and columns represent convective (a,c) and stratiform (b,d) features. The first row (a-b) are the observations from RELAMPAGO for each variable while the second (c-d) displays "PRE"-CIP.

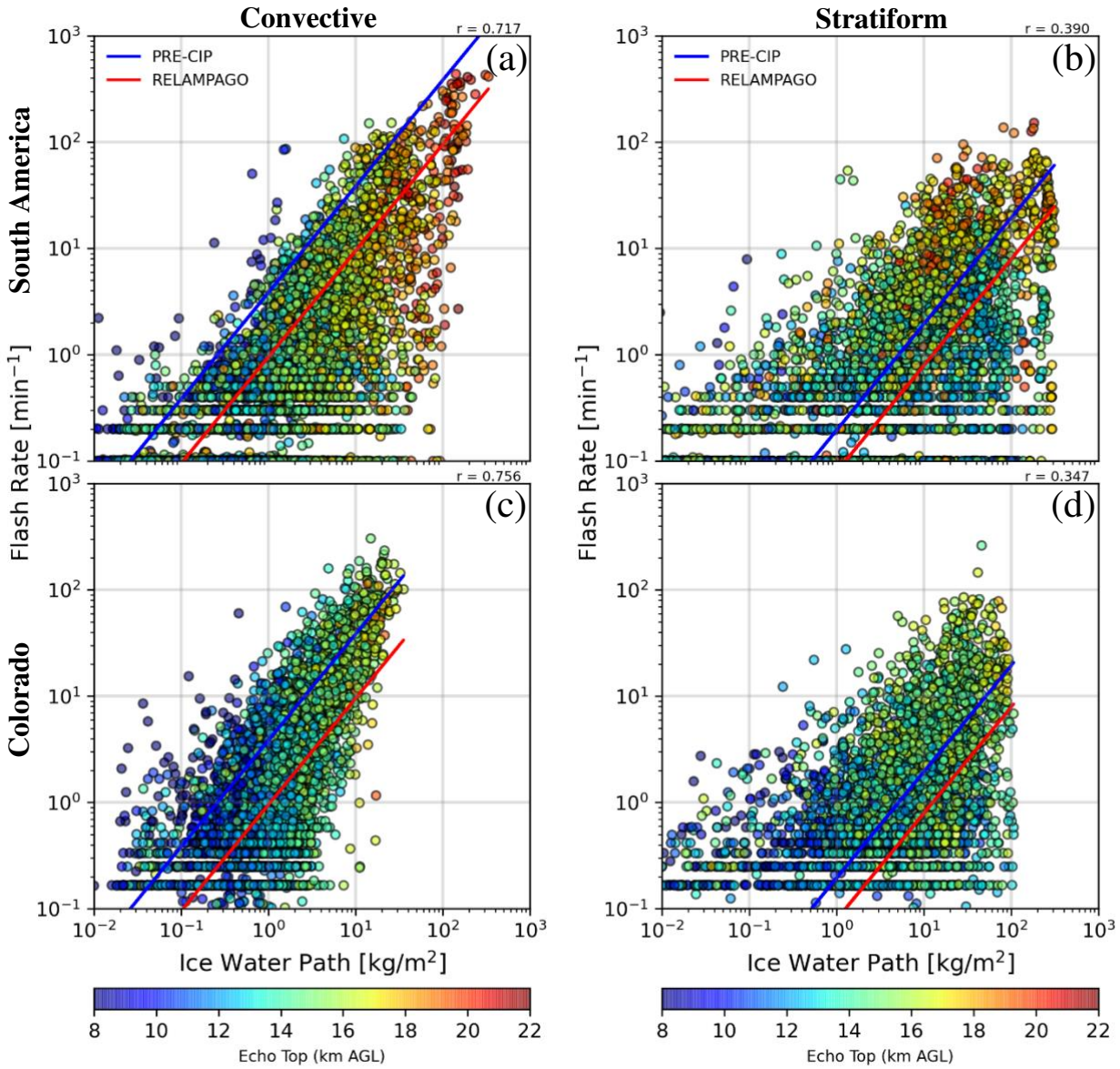

Figure 3.8: As in Fig. 3.7, but for ice water path (IWP) (kg / m^2).

Separating features into convective or stratiform precipitation allows us to focus on specific differences between the archetypes. Convective features clearly show a preference for higher echo top heights as 35 dBZ volume (Fig. 3.7a, c) or IWP increases (Fig. 3.8a, c) in both regions, with higher echo top heights as lightning flash rates increase. Stratiform features show a different distribution, with echo top heights appearing widely throughout the distribution (Figs. 3.7b, d; 3.8b, d), making echo top height less of an important predictor for lightning flash rates. Related to

this, stratiform features have greater spread than convective features in both regions, particularly in SSA, and especially for IWP. In the previous section, IWP had the lowest r-score of the lightning regressions (Fig. 3.5b, d) and Figures 3.8b and d show that it may be related to a weaker relationship between IWP and lightning flashes in stratiform regions for both campaigns. The Steiner et al. (1995) partitioning allows us to be more detailed in our regression creation, separating features that should not be treated as a single unified category, but instead as unique precipitation regions that deserve their own examination.

3.4 TRMM-heritage Storm Mode Regressions

As valuable as convective/stratiform partitioning is in separating lightning characteristics by different types of precipitation, one additional level of partitioning is done to examine extreme storms through the use of TRMM-heritage storm modes. As discussed previously, SSA is characterized by frequent upscale growth over the SDC and in the Andes foothills, leading to systematically larger and taller storms than seen in Colorado (Figs. 3.1 and 3.2, Table 2.1). For simplicity, we group DCC and DWCC features together for this analysis, treating them as one unified "deep" category as has been done in prior studies (Romatschke and Houze 2010; Rasmussen and Houze 2011). Yet again, similar themes persist in Figures 3.9 and 3.10 as before (Figs 3.5-3.8), with the Colorado regressions having higher r-values due to a tighter distribution of features, and a consistently less steep regression from RELAMPAGO.

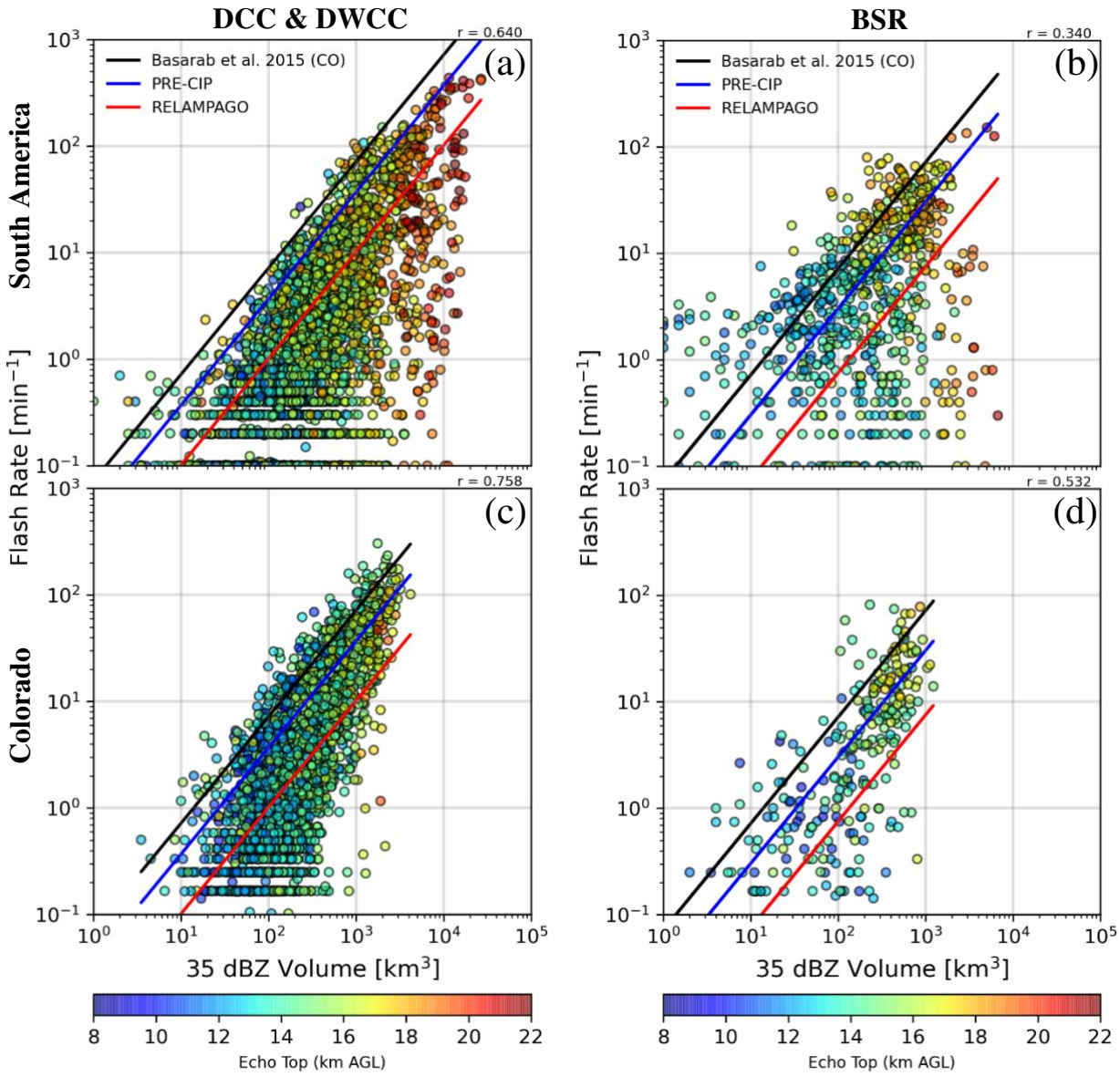

Figure 3.9: As in Fig. 3.7, but columns represent broad stratiform (BSR) storm mode features (b,d) and the combination of deep convective (DCC) and deep and wide convective (DWCC) features (a,c). All panels are scatter plots of lightning flash rates (min^{-1}) vs. total 35 dBZ volume (km^3), with formatting as in all prior.

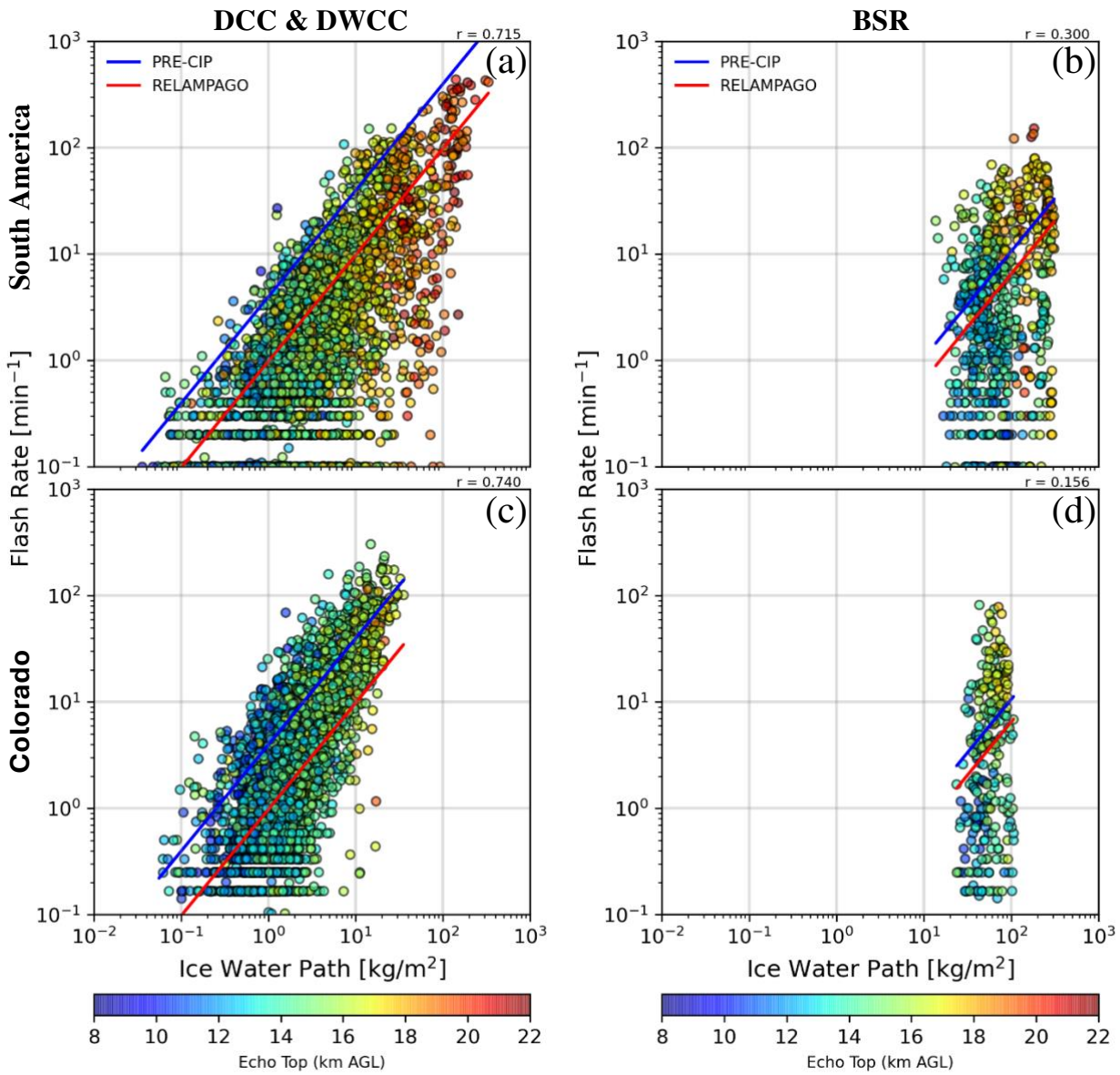

Figure 3.10: As in Fig. 3.8, but columns represent broad stratiform (BSR) storm mode features (b,d) and the combination of deep convective (DCC) and deep and wide convective (DWCC) features (a,c). All panels are scatter plots of lightning flash rates (min^{-1}) vs. ice water path (IWP) (kg / m^2), with formatting as in all prior.

Recall that IWP captures all ice hydrometeors within a feature, regardless of proximity to the mixed phase region where electrification occurs. This parameter has clear weakness for both stratiform and BSR features, as they may be influenced by ice processes far removed from the primary convective updraft that drives electrification. However, IWP regressions show relatively

strong correlations to lightning flash rates within convective and DCC/DWCC features, highlighting the importance of partitioning PFs into more characteristic sub-features in developing accurate parameterizations.

Analysis of the full spectrum of electrically-active storms across an entire warm-season in two regions allows us to examine how electrification processes differ across these two domains, and how there is a systematic difference in regression performance and behavior. Storms in SSA consistently require greater 35 dBZ and graupel volumes to produce similar flash rates as storms from Colorado, across all levels of partitioning. These results suggest characteristic differences in electrification processes and efficiency between these regions, while also demonstrating the variability within each given region. Table 3.2 summarizes the linear regression equations for some of the best performing parameters for PFs across both regions.

Table 3.2: Table summarizing the PF linear regression equations predicting lightning flash rate based on 35 dBZ volume (km^3), graupel volume (GRV, km^3), graupel mass (GRM, kg), and ice water path (IWP, kg m^{-2}) for both "PRE"-CIP and RELAMPAGO datasets.

	Colorado Equation	**SSA Equation**
35 dBZ (km^3)	$F = (3.9 \times 10^{-2}) \times 35\ dBZ$	$F = (9.3 \times 10^{-3}) \times 35\ dBZ$
GRV (km^3)	$F = (3.3 \times 10^{-2}) \times GRV$	$F = (9.7 \times 10^{-3}) \times GRV$
GRM (kg)	$F = (1.4 \times 10^{-8}) \times GRM$	$F = (3.6 \times 10^{-9}) \times GRM$
IWP (kg / m^2)	$F = (9.8 \times 10^{-1}) \times IWP$	$F = (2.7 \times 10^{-1}) \times IWP$

3.5 Warm Cloud Depth / Flash Heights

The final portion of this analysis examines campaign-wide characteristics of dominant charging process differences between our two regions. Recall that charging polarity is dependent on supercooled liquid water content and temperature within the mixed phase region, where NIC processes occur (Saunders et al. 2006). Transport of supercooled liquid water is driven by the strength of the updraft as well as the vertical extent of the WCD, defined as the region of a cloud between the lifting condensation level (LCL) and the freezing level. Thicker WCDs increase residence time within their above-freezing environment and an increase in collision-coalescence processes, forcing the increased rate of rain formation and a decrease in supercooled liquid water transport to the mixed phase region. Storms develop anomalous polarities when graupel becomes positively charged due to faster depositional growth in environments with greater supercooled liquid water, resulting in a net negative charge transfer to the colliding ice crystal, suggesting that shallower WCDs are a crucial ingredient for anomalous charging process (Emersic and Saunders 2010, Fuchs et al. 2018, Fuchs and Rutledge 2018). Figure 3.11 (WCD) shows the frequency of sounding-derived warm cloud depths for all lightning-producing PFs from both campaigns.

Systematically shallower WCDs from “PRE”-CIP highlight the more arid environment of northern Colorado, where climatologically drier air dominates. Approximately 9% of LCL heights calculated from “PRE”-CIP soundings were above the environmental freezing level, meaning there was no appreciable WCD. This is in clear contrast to the more moist environment of SSA fueled by the SALLJ, with systematically deeper WCDs and not a single instance of an LCL found above the freezing level. These fundamental differences in WCD and warm cloud processes suggest a

greater transport of supercooled liquid water into the mixed phase region in Colorado, likely leading to a greater proportion of anomalous polarity storms (Fuchs et al. 2018).

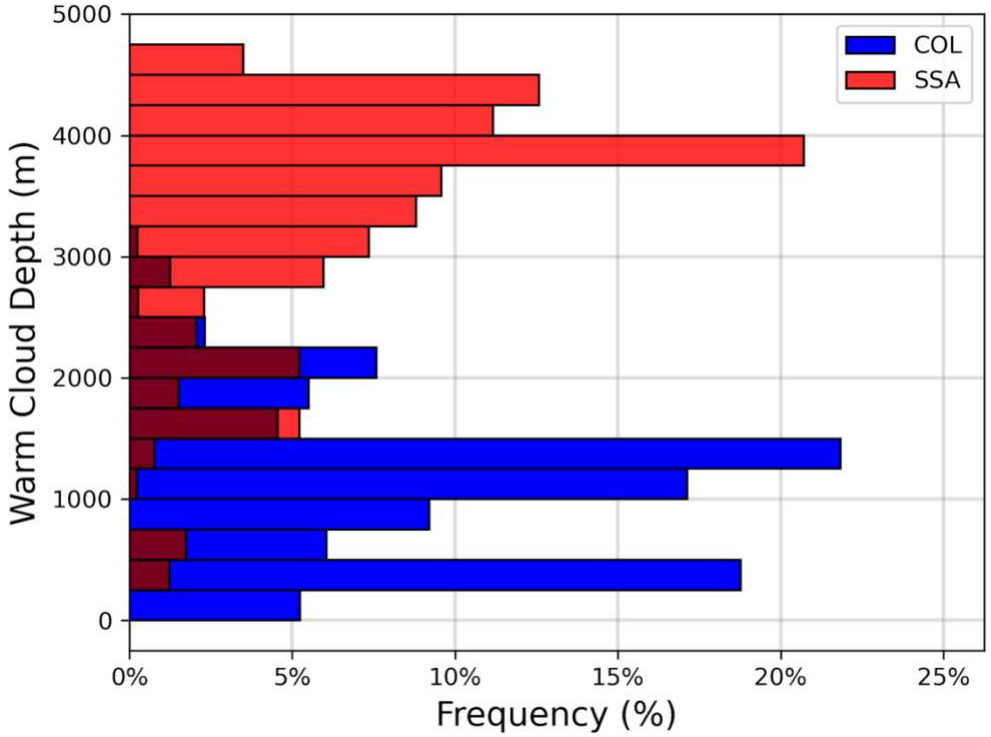

Figure 3.11: Frequency histograms of the warm cloud depth (WCD) for all PFs with lightning, determined by the distance between the sounding-calculated LCL and sounding-observed freezing level (0°C) height AGL, for both PFs from RELAMPAGO (red) and "PRE"-CIP (blue). In instances where the LCL was above the freezing level, WCD was not calculated.

Additional comparisons of lightning flash heights and temperatures (Figure 3.12) demonstrate how flashes preferentially occurred at lower heights and warmer temperatures during "PRE"-CIP compared to RELAMPAGO, with Colorado flashes often occurring nearly 4 km lower and 15° C colder than in SSA on average.

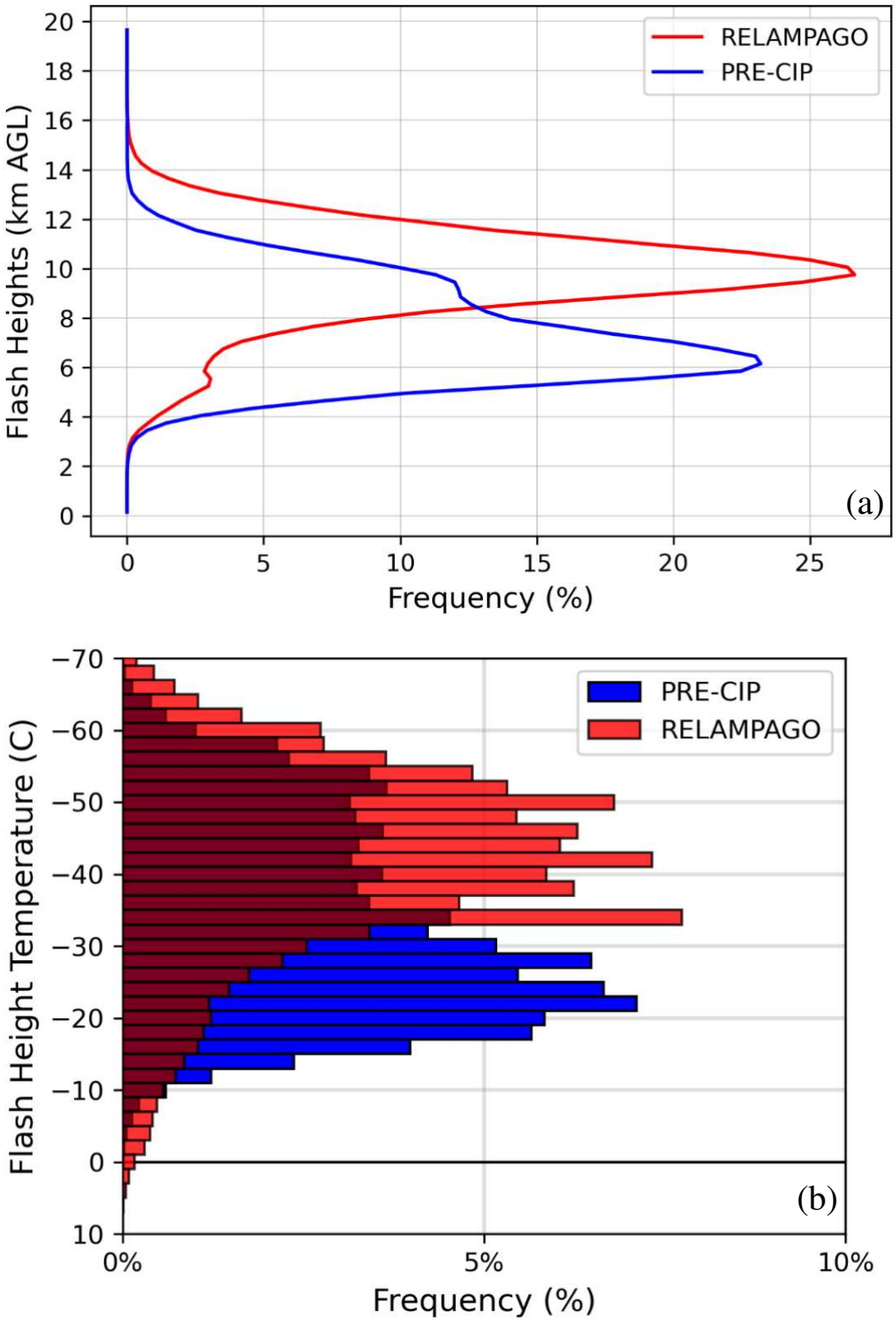

Figure 3.12: Probability distribution functions (PDFs) of lightning flash centroid altitudes (m AGL) (a) and frequency histograms of sounding-derived temperatures (b) from RELAMPAGO (SSA, red) and Colorado (COL, blue). Only flashes associated with a PF are included.

While we do not directly measure or identify storm polarity in this work, results from Medina et al. (2021) found that only 13.3% of storms from RELAMPAGO had anomalous polarity, compared to 82.6% from Colorado storms. Anomalous polarity storms preferentially produce lightning at lower elevations, likely explaining the dominant flash height differences between regions. Additionally, both PDFs in Figure 3.12 have clear secondary probability maximums near 9 km for Colorado and 6 km for SSA. This is likely a signal of the presence of non-dominant polarity flashes in each region, with the less common anomalous storms in SSA producing lower elevation flashes and the normal polarity storms in Colorado producing higher elevation flashes. This interpretation agrees with results found in Lang et al. (2020), which found a secondary peak of RELAMPAGO flash heights near 6 km that they attributed to anomalously polarized storms and stratiform lightning.

Chapter 4

CONCLUSIONS AND FUTURE WORK

This study presents an unprecedented opportunity to directly compare ground-based radar and LMA observations from Colorado and subtropical South America. For the first time, two warm-season, multi-instrumental datasets from the RELAMPAGO and 'PRE'-CIP field campaigns were analyzed side by side, providing a unique chance to examine fundamental microphysical differences in storm electrification and lightning behavior across two regions marked by topographically driven convection and distinct lightning activity. Critical for the accuracy and confidence of this comparison was the consistency in datasets utilized, developed with uniquely similar instrumentation and methodologies, with the intentional co-location of the CSU-CHIVO radar, LMAs, and radiosonde launches in both regions. Linear regressions were created between radar-observed and derived microphysical parameters and LMA-observed lightning flash rates across the complete spectrum of lightning-producing storms for both Colorado and subtropical South America. Additionally, spatial lightning climatologies and environmental processes critical to electrification and storm polarity were examined.

These comparisons help confirm that lightning regressions and environmental drivers of electrification have significant variability across distinct regions as well as within a single region, in contrast to results from Petersen et al. (2005) that suggested a regionally invariant relationship between lightning flash rates and IWP. SSA storms require significantly more graupel and intense echoes to produce the same lightning flash rate as an equivalent storm in Colorado, yet convective, stratiform, DCC, DWCC, and BSR partitioning of storm features manifest this relationship at different magnitudes. Relationships must be developed for discrete storm types both within and

across regions to account for the significant variability observed across the entire spectrum of storm behavior. Despite these critical differences across regions and storm modes, the 35 dBZ volume parameter is consistently amongst the strongest predictor of resultant lightning in both campaign datasets, even when compared to more sophisticated HID-derived parameters, suggesting that well-performing lightning regressions can be created in regions without dual-polarization-capable radar coverage and complex HID and Z-M ratio assumptions. It is not clear to what extent storm polarity contributes to the differences seen in flash rate regressions, warranting a more detailed investigation into the role of the environment on storm-by-storm charging processes.

A conceptual model is developed (Figure 4.1) to summarize the key results from this study that characterize a hypothetical representative storm from each region, in which both produce an equivalent flash rate. For a subtropical South American storm to match the flash rate of a storm observed in the Colorado plains, it will have a taller echo top height, greater 35 dBZ volume, thicker WCD, and higher lightning flash heights. In addition, the SSA storm occurs in an environment with a taller parent mountain range and resultant stronger CIN and CAPE compared to lower mountain ranges (Rasmussen and Houze 2016). The SSA storm will be larger and wider, likely initiating over the SDC before moving east, with a strong chance of exhibiting back-building along the mountains throughout its lifecycle.

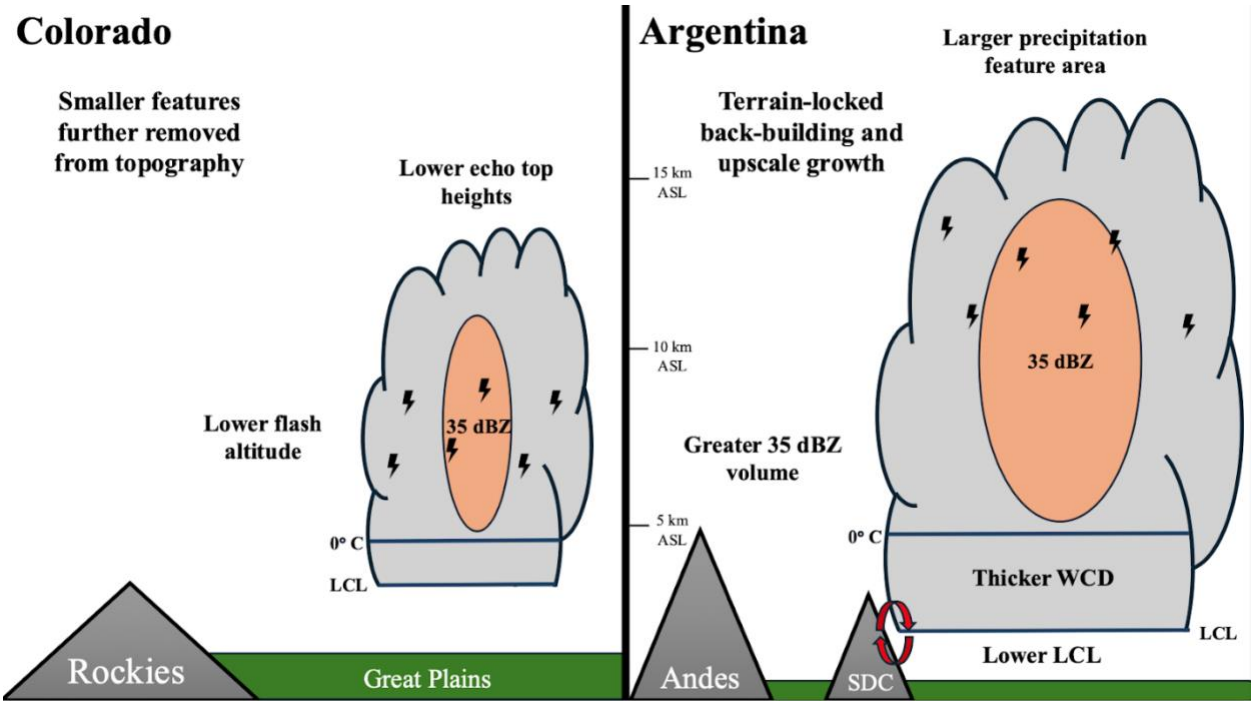

Figure 4.1: Conceptual model of the defining characteristics of storms from both regions. Terrain height and storm characteristics are depicted relative to the vertical height axis.

The characteristic differences in convective processes and resultant lightning behavior identified between these two regions demonstrates the need for future work to prioritize both microphysical and kinematic drivers of electrification in a more diverse sample of climate regions around the world. The first spaceborne observations of Convective Mass Flux (CMF) from the upcoming Investigation of Convective Updrafts Satellite (INCUS; https://incus.colostate.edu/) will provide an additional platform and perspective to measure the effectiveness of kinematic updraft processes in regions without vertical motion measurements, allowing for observations across both well and under-sampled electrically active regions on Earth. Additionally, satellite observations of storm intensity, size, and lightning activity can be compared to reanalysis-derived environmental parameters to investigate how specific environmental regimes may influence storm mode development and resultant lightning behavior across climate regions without robust ground-based observational networks. These insights into global variability in convective and

electrification processes can inform and be applied to further understanding of how storm mode populations and resultant lightning may change in a future, warming climate.

REFERENCES

Albrecht, R. I., S. J. Goodman, D. E. Buechler, R. J. Blakeslee, and H. J. Christian, 2016: Where Are the Lightning Hotspots on Earth? *Bulletin of the American Meteorological Society*, **97**, 2051–2068, https://doi.org/10.1175/BAMS-D-14-00193.1.

Arias, I., V. Chandrasekar, and S. S. Joshil, 2019: Cross-Validation of CSU-Chivo Radar and GPM During Relampago. *IGARSS 2019 - 2019 IEEE International Geoscience and Remote Sensing Symposium*, IGARSS 2019 - 2019 IEEE International Geoscience and Remote Sensing Symposium, Yokohama, Japan, IEEE, 7586–7589.

Barth, M. C., and Coauthors, 2015: The Deep Convective Clouds and Chemistry (DC3) Field Campaign. *Bulletin of the American Meteorological Society*, **96**, 1281–1309, https://doi.org/10.1175/BAMS-D-13-00290.1.

Basarab, B. M., S. A. Rutledge, and B. R. Fuchs, 2015: An improved lightning flash rate parameterization developed from Colorado DC3 thunderstorm data for use in cloud-resolving chemical transport models. *JGR Atmospheres*, **120**, 9481–9499, https://doi.org/10.1002/2015JD023470.

Bell, M. M., 2022: nsf-lrose/lrose-topaz: lrose-topaz-20220222. https://doi.org/10.5281/ZENODO.6909479.

Bruick, Z. S., K. L. Rasmussen, and D. J. Cecil, 2019: Subtropical South American Hailstorm Characteristics and Environments. *Monthly Weather Review*, **147**, 4289–4304, https://doi.org/10.1175/MWR-D-19-0011.1.

Carbone, R. E., J. D. Tuttle, D. A. Ahijevych, and S. B. Trier, 2002: Inferences of Predictability Associated with Warm Season Precipitation Episodes. *J. Atmos. Sci.*, **59**, 2033–2056, https://doi.org/10.1175/1520-0469(2002)059<2033:IOPAWW>2.0.CO;2.

Carey, L. D., E. V. Schultz, C. J. Schultz, W. Deierling, W. A. Petersen, A. L. Bain, and K. E. Pickering, 2019: An Evaluation of Relationships between Radar-Inferred Kinematic and Microphysical Parameters and Lightning Flash Rates in Alabama Storms. *Atmosphere*, **10**, 796, https://doi.org/10.3390/atmos10120796.

Cecil, D. J., and C. B. Blankenship, 2012: Toward a Global Climatology of Severe Hailstorms as Estimated by Satellite Passive Microwave Imagers. *Journal of Climate*, **25**, 687–703, https://doi.org/10.1175/JCLI-D-11-00130.1.

Chmielewski, V. C., and E. C. Bruning, 2016: Lightning Mapping Array flash detection performance with variable receiver thresholds. *JGR Atmospheres*, **121**, 8600–8614, https://doi.org/10.1002/2016JD025159.

Deierling, W., and W. A. Petersen, 2008: Total lightning activity as an indicator of updraft characteristics. *J. Geophys. Res.*, **113**, 2007JD009598, https://doi.org/10.1029/2007JD009598.

Deierling, W., W. A. Petersen, J. Latham, S. Ellis, and H. J. Christian, 2008: The relationship between lightning activity and ice fluxes in thunderstorms. *J. Geophys. Res.*, **113**, 2007JD009700, https://doi.org/10.1029/2007JD009700.

Dolan, B., S. A. Rutledge, S. Lim, V. Chandrasekar, and M. Thurai, 2013: A Robust C-Band Hydrometeor Identification Algorithm and Application to a Long-Term Polarimetric Radar Dataset. *Journal of Applied Meteorology and Climatology*, **52**, 2162–2186, https://doi.org/10.1175/JAMC-D-12-0275.1.

Emersic, C., and C. P. R. Saunders, 2010: Further laboratory investigations into the Relative Diffusional Growth Rate theory of thunderstorm electrification. *Atmospheric Research*, **98**, 327–340, https://doi.org/10.1016/j.atmosres.2010.07.011.

Fuchs, B. R., and S. A. Rutledge, 2018: Investigation of Lightning Flash Locations in Isolated Convection Using LMA Observations. *JGR Atmospheres*, **123**, 6158–6174, https://doi.org/10.1002/2017JD027569.

Fuchs, B. R., S. A. Rutledge, B. Dolan, L. D. Carey, and C. Schultz, 2018: Microphysical and Kinematic Processes Associated With Anomalous Charge Structures in Isolated Convection. *JGR Atmospheres*, **123**, 6505–6528, https://doi.org/10.1029/2017JD027540.

Houze, R. A., 2004: Mesoscale convective systems. *Reviews of Geophysics*, **42**, 2004RG000150, https://doi.org/10.1029/2004RG000150.

Houze, R. A., K. L. Rasmussen, M. D. Zuluaga, and S. R. Brodzik, 2015: The variable nature of convection in the tropics and subtropics: A legacy of 16 years of the Tropical Rainfall Measuring Mission satellite. *Reviews of Geophysics*, **53**, 994–1021, https://doi.org/10.1002/2015RG000488.

Insel, N., C. J. Poulsen, and T. A. Ehlers, 2010: Influence of the Andes Mountains on South American moisture transport, convection, and precipitation. *Clim Dyn*, **35**, 1477–1492, https://doi.org/10.1007/s00382-009-0637-1.

Kummerow, C., W. Barnes, T. Kozu, J. Shiue, and J. Simpson, 1998: The Tropical Rainfall Measuring Mission (TRMM) Sensor Package. *J. Atmos. Oceanic Technol.*, **15**, 809–817, https://doi.org/10.1175/1520-0426(1998)015<0809:TTRMMT>2.0.CO;2.

Lang, T. J., and Coauthors, 2020: The RELAMPAGO Lightning Mapping Array: Overview and Initial Comparison with the Geostationary Lightning Mapper. *Journal of Atmospheric and Oceanic Technology*, **37**, 1457–1475, https://doi.org/10.1175/JTECH-D-20-0005.1.

Liu, C., D. J. Cecil, E. J. Zipser, K. Kronfeld, and R. Robertson, 2012: Relationships between lightning flash rates and radar reflectivity vertical structures in thunderstorms over the tropics and subtropics. *J. Geophys. Res.*, **117**, 2011JD017123, https://doi.org/10.1029/2011JD017123.

Medina, B. L., L. D. Carey, T. J. Lang, P. M. Bitzer, W. Deierling, and Y. Zhu, 2021: Characterizing Charge Structure in Central Argentina Thunderstorms During RELAMPAGO Utilizing a New Charge Layer Polarity Identification Method. *Earth and Space Science*, **8**, e2021EA001803, https://doi.org/10.1029/2021EA001803.

Mulholland, J. P., S. W. Nesbitt, R. J. Trapp, K. L. Rasmussen, and P. V. Salio, 2018: Convective Storm Life Cycle and Environments near the Sierras de Córdoba, Argentina. *Monthly Weather Review*, **146**, 2541–2557, https://doi.org/10.1175/MWR-D-18-0081.1.

Mulholland, J. P., S. W. Nesbitt, R. J. Trapp, and J. M. Peters, 2020: The Influence of Terrain on the Convective Environment and Associated Convective Morphology from an Idealized Modeling Perspective. *Journal of the Atmospheric Sciences*, **77**, 3929–3949, https://doi.org/10.1175/JAS-D-19-0190.1.

Nesbitt, S. W., and Coauthors, 2021: A Storm Safari in Subtropical South America: Proyecto RELAMPAGO. *Bulletin of the American Meteorological Society*, **102**, E1621–E1644, https://doi.org/10.1175/BAMS-D-20-0029.1.

Petersen, W. A., H. J. Christian, and S. A. Rutledge, 2005: TRMM observations of the global relationship between ice water content and lightning. *Geophysical Research Letters*, **32**, 2005GL023236, https://doi.org/10.1029/2005GL023236.

Piersante, J. O., K. L. Rasmussen, R. S. Schumacher, A. K. Rowe, and L. A. McMurdie, 2021: A Synoptic Evolution Comparison of the Smallest and Largest MCSs in Subtropical South America between Spring and Summer. *Monthly Weather Review*, https://doi.org/10.1175/MWR-D-20-0208.1.

Proctor, D. E., 1971: A hyperbolic system for obtaining VHF radio pictures of lightning. *J. Geophys. Res.*, **76**, 1478–1489, https://doi.org/10.1029/JC076i006p01478.

Rasmussen, K. L., and R. A. Houze, 2011: Orogenic Convection in Subtropical South America as Seen by the TRMM Satellite. *Monthly Weather Review*, **139**, 2399–2420, https://doi.org/10.1175/MWR-D-10-05006.1.

Rasmussen, K. L., and R. A. Houze, 2016a: Convective Initiation near the Andes in Subtropical South America. *Monthly Weather Review*, **144**, 2351–2374, https://doi.org/10.1175/MWR-D-15-0058.1.

Rasmussen, K. L., and R. A. Houze, 2016b: Convective Initiation near the Andes in Subtropical South America. *Monthly Weather Review*, **144**, 2351–2374, https://doi.org/10.1175/MWR-D-15-0058.1.

Rasmussen, K. L., M. D. Zuluaga, and R. A. Houze, 2014: Severe convection and lightning in subtropical South America. *Geophysical Research Letters*, **41**, 7359–7366, https://doi.org/10.1002/2014GL061767.

Rasmussen, K. L., M. M. Chaplin, M. D. Zuluaga, and R. A. Houze, 2016: Contribution of Extreme Convective Storms to Rainfall in South America. *Journal of Hydrometeorology*, **17**, 353–367, https://doi.org/10.1175/JHM-D-15-0067.1.

Reynolds, S. E., M. Brook, and M. F. Gourley, 1957: THUNDERSTORM CHARGE SEPARATION. *J. Meteor.*, **14**, 426–436, https://doi.org/10.1175/1520-0469(1957)014<0426:TCS>2.0.CO;2.

Rison, W., R. J. Thomas, P. R. Krehbiel, T. Hamlin, and J. Harlin, 1999: A GPS-based three-dimensional lightning mapping system: Initial observations in central New Mexico. *Geophysical Research Letters*, **26**, 3573–3576, https://doi.org/10.1029/1999GL010856.

Rocque, M. N., and S. A. Rutledge, 2021: Diurnal Cycle of Precipitation Features Observed during DYNAMO. *Journal of the Atmospheric Sciences*, **78**, 2287–2306, https://doi.org/10.1175/JAS-D-20-0215.1.

Rocque, M. N., and K. L. Rasmussen, 2022: The Impact of Topography on the Environment and Life Cycle of Weakly and Strongly Forced MCSs during RELAMPAGO. *Monthly Weather Review*, **150**, 2317–2338, https://doi.org/10.1175/MWR-D-22-0049.1.

Rocque, M. N., W. Deierling, K. L. Rasmussen, R. I. Albrecht, and B. L. Medina, 2024: Lightning Characteristics Associated With Storm Modes Observed During RELAMPAGO. *JGR Atmospheres*, **129**, e2023JD039520, https://doi.org/10.1029/2023JD039520.

Romatschke, U., and R. A. Houze, 2010: Extreme Summer Convection in South America. *Journal of Climate*, **23**, 3761–3791, https://doi.org/10.1175/2010JCLI3465.1.

Rutledge, S. A., K. A. Hilburn, A. Clayton, B. Fuchs, and S. D. Miller, 2020: Evaluating Geostationary Lightning Mapper Flash Rates Within Intense Convective Storms. *JGR Atmospheres*, **125**, e2020JD032827, https://doi.org/10.1029/2020JD032827.

Sasaki, C. R. S., A. K. Rowe, L. A. McMurdie, A. C. Varble, and Z. Zhang, 2024: Influences of the South American Low-Level Jet on the Convective Environment in Central Argentina Using a Convection-Permitting Simulation. *Monthly Weather Review*, **152**, 629–648, https://doi.org/10.1175/MWR-D-23-0122.1.

Saunders, C. P. R., H. Bax-norman, C. Emersic, E. E. Avila, and N. E. Castellano, 2006: Laboratory studies of the effect of cloud conditions on graupel/crystal charge transfer in thunderstorm electrification. *Quart J Royal Meteoro Soc*, **132**, 2653–2673, https://doi.org/10.1256/qj.05.218.

Schumacher, R. S., and Coauthors, 2021: Convective-Storm Environments in Subtropical South America from High-Frequency Soundings during RELAMPAGO-CACTI. *Monthly Weather Review*, **149**, 1439–1458, https://doi.org/10.1175/MWR-D-20-0293.1.

Singh, I., S. W. Nesbitt, and C. A. Davis, 2022: Quasi-Idealized Numerical Simulations of Processes Involved in Orogenic Convection Initiation over the Sierras de Córdoba. *Journal of the Atmospheric Sciences*, **79**, 1127–1149, https://doi.org/10.1175/JAS-D-21-0007.1.

Steiner, M., R. A. Houze, and S. E. Yuter, 1995: Climatological Characterization of Three-Dimensional Storm Structure from Operational Radar and Rain Gauge Data. *J. Appl. Meteor.*, **34**, 1978–2007, https://doi.org/10.1175/1520-0450(1995)034<1978:CCOTDS>2.0.CO;2.

Vera, C., and Coauthors, 2006: The South American Low-Level Jet Experiment. *Bull. Amer. Meteor. Soc.*, **87**, 63–78, https://doi.org/10.1175/BAMS-87-1-63.

Vivekanandan, J., S. M. Ellis, R. Oye, D. S. Zrnic, A. V. Ryzhkov, and J. Straka, 1999: Cloud Microphysics Retrieval Using S-band Dual-Polarization Radar Measurements. *Bull. Amer. Meteor. Soc.*, **80**, 381–388, https://doi.org/10.1175/1520-0477(1999)080<0381:CMRUSB>2.0.CO;2.

Williams, E. R., R. Zhang, and J. Rydock, 1991: Mixed-Phase Microphysics and Cloud Electrification. *J. Atmos. Sci.*, **48**, 2195–2203, https://doi.org/10.1175/1520-0469(1991)048<2195:MPMACE>2.0.CO;2.

Zipser, E. J., D. J. Cecil, C. Liu, S. W. Nesbitt, and D. P. Yorty, 2006: WHERE ARE THE MOST INTENSE THUNDERSTORMS ON EARTH? *Bull. Amer. Meteor. Soc.*, **87**, 1057–1072, https://doi.org/10.1175/BAMS-87-8-1057.